Developing a Design Procedure for Cross Laminated Timber Mats

BY

Ines Torra
B.S., University of Illinois at Chicago, Chicago, 2015

THESIS

Submitted as partial fulfillment of the requirements
For the degree of Master of Science in Civil Engineering
In the Graduate College of the
University of Illinois at Chicago, 2017

Chicago, Illinois

Defense Committee:

Dr Mustafa Mahamid, Advisor, Civil and Materials Engineering
Dr Eduard Karpov, Chair, Civil and Materials Engineering
Dr Michael McNallan, Civil and Materials Engineering

ACKNOWLEDGMENTS

I would like to express the deepest appreciation to my advisor, Dr Mustafa Mahamid, for his outstanding support and guidance. He is an icon of leadership and intellect and without his persistent help and supervision, this research would have not been possible. I consider it an honor to have been Dr Mahamid's graduate student.

I would like to genuinely thank my fiancée, Kamel Bilal for his endless support, patience and encouragement throughout my Master's Degree. Despite my academic career's many twists and turns, he pushed me to move forward, always believed in me and I would have not gotten here without him.

I would also like to show my gratitude to my parents who live overseas, who never stopped motivating me in completing this degree. Thank you, Mom and Dad for your continuous support of me pursuing my dreams.

Additionally, I would like to thank my labmate, Ata Taghipour, for his support and many other friends and family members who were always there for me.

TABLE OF CONTENTS

LIST OF TABLES

LIST OF FIGURES

LIST OF FIGURES (continued)

SUMMARY

A study on the behavior and design of Cross Laminated Timber (CLT) Mats was carried out using the finite element software ANSYS. The finite element models were validated with experimental results done by other researchers. The validation was achieved by comparing load displacement curves of the Finite Element Analysis (FEA) results vs experimental results of a 5 ply CLT mat composed of Southern Yellow Pine (SYP) No. 2 grade, under four-point bending test.

A comparison was carried out between the behavior of wood traditional mats connected by steel rods and different configurations of CLT mats. The comparison was performed between 5 ply and 7 ply CLT mats and a 12 in thick traditional wood members consisting of 4 1" diameter A36 steel rods placed along the length of mat. All models are made of Southern Yellow Pine (SYP) No.2 grade and simply supported boundary conditions were provided.

A design procedure was developed based on previous published guidelines for mobile crane mats and the Shear Analogy Method used in the CLT Handbook. Due to its unique arrangement, CLT's effective section properties should be investigated and calculated. Recommendations have been made on the design procedure of such members.

CHAPTER 1: INTODUCTION

1.1. Background

Cross-laminated timber (CLT), a new generation of engineered wood product developed initially in Europe, is a relatively innovative building system of interest in the North American construction and is helping to define a new class of timber products known as massive or "mass" timber. CLT members consist of several layers of lumber boards stacked crosswise (typically 90 degrees) and glued together on their wide faces and sometimes, on the narrow faces as well. A cross section of a CLT element has at least three glued layers of boards placed in orthogonally alternating orientation to the neighboring layers. CLT products are usually consist an odd number of layers: three to seven layers usually and even more in some cases. The thickness of individual lumber member varies from 5/8 inch to 2.0 inches [1]. Figure 1 illustrates a typical 5-ply CLT panel configuration [1].

Figure 1: 5-ply typical CLT panel configuration

Being introduced in the early 1990s in Austria and Germany [1], this material has been gaining popularity in residential and non-residential applications in several countries. Numerous impressive low- and mid-rise buildings and other structures built around the world using CLT show the many advantages that this product can offer to the construction industry. Some of its beneficial characteristics are: high dimension stability, high strength and stiffness, easily

manufactured, fire resistant, cost and energy efficient, renewable and biodegradable, composed of lighter panels which lead to smaller foundations, sustainable, carbon sink and good thermal and sound insulating properties. However, wood represents a very complicated material whose behavior is difficult to predict in various applications and requires care from the engineering community. It is apparent that our knowledge, although greatly advanced in recent years, still lacks in several areas of wood research. A lot of material failures in wood structures have occurred in the past due to lack of structural checks, construction mistakes or wrong calculation of loads. For example, failure of CLT mats used as temporary bridges over rivers have led to death of construction workers and other catastrophic incidents, which creates an urgent need to use better and more innovative techniques in wood design research. Although experimentation must be primary to progress in this field, it must be coupled with more essential studies at the theoretical level, such as simulation, which can be for different conditions and configurations.

In this study, we propose to develop a non-linear finite element model for Cross-Laminated Timber mats and study their behavior and failure modes. This research entails of two stages: the first stage involves the development of a CLT model using the powerful finite element analysis tool, ANSYS and investigation of its linear and non-linear behavior. These findings will be verified based on experimental data previously performed at Forest Product Laboratory (FPL) in Madison, WI. After proving the effectiveness of this model, CLT Mats supported by soil are analyzed. This study enables the prediction of CLT and soil behavior up to failure which will lead to more realistic simulations of the materials. Using Finite Element Analysis to model and analyze CLT mats supported by soil will result in safer, better and more cost-efficient applications of this material in structural engineering.

1.2. Literature Review

Previous studies investigated the behavior and non-linear analysis of Cross Laminated Timber, experimentally and numerically and soil modeling and behavior. Some of these studies are described below:

Moses and Prion (2002) [21] investigated the anisotropic plasticity and failure prediction in wood composites. The Finite Element Analysis tool, ANSYS, was used to model the material non-linearities and failure mode. Yield and post yield behavior of wood composites were achieved based on the predicted stress distribution from the material model. The linear elastic orthotropic model and anisotropic plasticity options were used to predict the ultimate strength in wood. The material model was verified using two cases: the ASTM D143 shear block test and a single bolted connection and load displacement curves were plotted and compared with experimental results. This model is based on Hill's yield criterion for orthotropic materials and assumes equal tension and compression yield stresses for each direction of normal stress and tension behavior follows bi-linear stress-strain curve. As a result, the load displacement curves showed a good agreement with the experimental data and the predicted ultimate load due to shear or tension failure were reported for the shear block as well as the failure data for single bolt connection loaded perpendicular to grain and 45 degrees to grain. It was concluded from this study that the shear strength of wood in the primary shear planes could be determined from the shear block finite element model and the sensitivity analysis of connection behavior as well as material properties help in determining which material variables are most important in the production of wood composites.

Mahamid et al. (2017) [2] performed experiments and numerical modeling of CLT members by testing 20 specimens in bending and 20 specimens in shear to obtain the characteristic design values of F_b and F_v of CLT members with unique arrangements of Southern Yellow Pine (SYP) No. 2 grade. The specimens were loaded up to failure and the elastic and inelastic parameters of CLT were discussed. Load deflection curves were obtained from experiments. Non-linear Finite Element Analysis was performed to validate the results. The bending and shear strength parameters of CLT members were obtained and recommendations were made on how to design such members.

Hindman and Lee (2007) [20] investigated the effect of considering wood strands as two layer composites consisting of earlywood and latewood or intra-ring layers in their research: "Modeling wood strands as Multi-Layer Composites: Bending and Tension Loads". This study focuses on modeling wood as non-uniform heterogeneous material combining both latewood and earlywood effects which have different mechanical properties. Various specimen of earlywood and latewood were tested under tension and bending loads and several finite element models were created to predict the stiffness of wood strands and to compare two different kinds of models: homogenous and composite wood. As a conclusion, the composite wood shows a better agreement and more realistic model compared to the homogenous wood.

Mackerle (2005) [23] gives a bibliographical review of finite element analyses in wood research. This summary contains 300 references to papers and conference proceedings on the subject that were published between 1995 and 2004 that focus on wood as a construction material and wood structures and products. Some of the topics investigated are: material and mechanical properties of wood products and structures: lumber, glulam, panels, trusses and frames, floors, roofs, bridges, wood joining and fastening, drying process and thermal properties, fracture

mechanics issues and finite element methods applied to wood. This review helped gather more sources on the topics of interest.

O'Brien (2003) [24] investigated the behavior of wood and composite structured hockey sticks (typically made of wood, aluminum, or fiberglass). The main objective of this study was to understand the nature of the construction of wood and composite shafts and optimally design the dimensions necessary to handle various induced stresses by using an orthotropic material model and finite element analysis. This was a linear elastic study that used ANSYS as a main finite element tool to model and optimize the wood shaft. It was concluded from this study that composite wood shafts can resist high pressure without plastic deformation that allows manufacturers to model the shafts as hollow which is lightweight and durable.

CLT Handbook US Edition (2013) [1] published by FPInnovations describes in detail Cross Laminated Timber as a material, its properties, manufacturing process, structural and lateral design, connections in CLT buildings, vibration, fire and environmental performance in timber panels, floors and assemblies. This handbook provides an analytical and experimental overview of Cross Laminated Timber, its main key advantages and its behavior in general. One important aspect of this handbook used for the purpose of this study is the analytical design methods of CLT elements. The main method used for CLT design is the Shear Analogy Method from which can be obtained the bending and shear stiffness properties. This technique explains in detail how to determine effective stiffness properties of a composite section.

Duerr (2015) [7] described the analysis and design procedure for mobile crane mats in his book "Mobile Crane Support Handbook". The purpose of this handbook is to present mobile crane support design procedures that utilize practical soil and mat properties and that account for the

interaction between mats and soil, thus providing a more reliable and realistic design. Topics covered include support reactions from crawler and outrigger-supported cranes, soil bearing capacity, analysis of subsurface structures, strength of crane mats, practical design methods, and industry standards and regulations. The design of a crane mat requires a determination of the loads from the crane, an assessment of the bearing capacity of the soil, an assessment of the strength of mats (usually timber) and a calculation of the area of the mat that bears on the surface and contributes to the support of the crane. This handbook describes different design methods on how to analyze alternate mat arrangements supported by soil. Three main methods are described: mat length based on ground bearing capacity, mat length based on mat strength and balanced mat analysis method. All these methods are used to analyze the behavior of crane mats supported by soil. Duerr emphasizes in his book that laminated mats are not useful as crane mats due to limited strength and stiffness in bending which makes them rarely adequate for mobile crane support.

Tankut et al. (2014) [22] gave a bibliographical review of the finite element analysis of wood material applied to wooden furniture. Finite element analysis is recommended as a better method to use in furniture design compared to statistical methods of furniture optimization. The main steps of finite element method are described: preprocessing phase, solution phase and post processing phase. Further the role of FEA in wooden furniture design is emphasized: lowering manufacturing costs. A lot of different academic research papers are gathered and described to stress the importance of Finite Element Analysis Tools in wood and its applications.

Colakoglu and Apay (2012) [25] analyzed the behavior of a wooden chair simulated by free drop using finite element analysis. The analysis was performed for different kinds of wood: southern red oak, pine red and spruce Engelmann. The free drop test was initiated from two different heights. The wooden materials properties were taken and derived from Wood Handbook

of USDA Forest Product Laboratory, the free drop test was performed according to test standards of packaged furniture. The strength at different parts of the wooden chair was recorded and recommendations were made to furniture manufacturers and designers in order to minimize manufacturing costs. The FEA technique proved that the drop performance test is a time consuming and conservative procedure. Using Finite Element Analysis results in safer and cost effective design.

Stoeckel et al. (2013) [27] summarized and discussed the state of art of the mechanical properties of pure wood adhesives. Conventionally, mechanical adhesive properties were characterized by means of macroscopic tensile or bending tests of ex-situ cured adhesive films. More recently, nanoindentation was also used to characterize such ex-situ specimens, this method allows the mechanical characterization of adhesive bond lines in-situ. Mechanical tests revealed high variability between, but notably also within specific groups of adhesives. For example, the modulus of elasticity falls in a wide range from 0.1 GPa up to 15 GPa. The mechanical properties of adhesives are highly influenced by the material formation and environmental conditions such as moisture as well as by sample preparation and test method.

Adams et al. (1997) [28] provide a guide to adhesive joints within structures, especially those capable of bearing high loads in their book "Structural Adhesive Joints in engineering". The book covers all aspects of design, materials selection and testing, including the physical properties and cure-chemistry of structural adhesives and how to select adhesives for particular applications. An overall overview of properties of structural adhesives and their material behavior under different loads is provided in details analytically and experimentally. The stress-strain curves of different adhesives joints are shown in this book.

Guindos and Guaita (2012) [32] performed a parametric study using a three-dimensional wood material model using the finite element software ANSYS to predict the behavior of timber at the macro-scale considering the effect of any type of knot. Wood is considered a transversely isotropic material with anisotropic plasticity in which the failure prediction is given by means of several phenomenological failure criteria. The elastic and inelastic parameters of wood were discussed in detail and obtained from previous literature. After the validation of the model was completed, it was concluded that the model was validated with four point bending tests of Scots pine specimens showing errors in failure prediction of 5 %, errors in initial fracture location of less than 20 mm and errors of 9 % in photogrammetrically measured displacements of an average of 65 finite element nodes, in which the heterogeneity of wood caused variations of up to 6 %. This study has a big contribution to the heterogeneity of wood, allowing for wider and more realistic applications of this material.

Gillholm and Rosander (2014) [31] performed a study on how plastic mats deform and distribute stress on different soils in their research article "Evaluation of plastic mats as access roads"**.** The objective of this study is to examine the conditions required to use temporary plastic mats as access roads to wind farms. The plastic mats are analyzed with hand-calculations and a finite element analysis software: PLAXIS 2D and the behavior of the mat for different load and soil cases was investigated. Some of the aspects considered in this study are the mat deflection and load distribution and how that affects the soil system. The results show that the most sensitive parameters are the soil properties: angle of shear resistance for the non-cohesive soils, the undrained shear strength for clay, the groundwater level and the effective area of the road mat.

Wahab (2014) [19] performed an extensive study on how adhesives behave in composite and metal joints in his book "The Mechanics of Adhesives in Composite and Metal Joints". The

adhesives were considered as an elasto plastic material and the stress strain of different types of adhesives were developed. The mechanics of adhesives was studied using fracture mechanics and the finite element analysis commercial package, ANSYS. The theory behind modeling adhesives using ANSYS was investigated and discussed in detail. In addition, stress analysis, fracture and cohesive zone model analyses, crack propagation analysis and thermal and diffusion analyses were performed to reach conclusions about the behavior of adhesives in composite and metal joints.

Chi and Kushwaha (2013) [19] developed a nonlinear three-dimensional finite element model for a narrow cutting blade with different shapes. The authors focused on studying the soil forces on flat and triangular blades, the effect of tool curvature on soil surfaces and the comparison between the curved and flat tools using Finite Element Analysis. Soil was modeled as non-linear based on Kondner's model which is based on the equation of the tangent modulus. The soil parameters for nonlinear analysis were presented in this paper as well as the interface elements used between soil and the cutting blade. The results showed that the tool curvature angle has a significant effect in determining the soil forces. Increasing the curvature of the tool decreased the resistance of the soil movement and reduced the tillage draft.

Boldyrev and Muyzemnek (2008) [12] analyzed the modeling of deformation process in soils using finite element tools: ANSYS and LS-Dyna Programs. The soil was modeled using Drucker Prager failure criterion and all parameters were identified using the theory and equations of this principle in ANSYS. The soil was loaded with central and eccentric loads. The finite element results were compared against experimental data on which the required parameters of models were obtained. The numerical solution was performed using two different programs and results were compared. All soil parameters were identified and explained in detail and how they can be used to model soil nonlinearly using Drucker Prager principle.

Ravishankar and Satyam (2013) [30] investigated the behavior of a 150 m tall asymmetrical building with two different foundation systems such as raft and pile assuming homogenous sandy soil under dynamic loading. The input of Bhuj ground motion was used to investigate the response of structure in terms of Soil Structure Interaction (SSI) which explains why the tall asymmetric building are at higher risk during earthquakes. The soil was modeled nonlinearly using solid elements and Drucker Prager failure principle in ANSYS and the parameters used were presented in this study. The response was studied statically and dynamically. Displacements in all directions were plotted against time and maximum displacements and stresses were recorded under dynamic loading for both raft and pile foundation system.

1.3. Research Significance and Scope

Wood is known to be one of the most complicated raw materials. It is apparent that this material reflects very complicated behavior and that little research has been conducted to further explore the behavior of this material characterized by many advantages. The proposed non-linear finite element model supported by soil is ideally suited to analyze and predict this complex material behavior that will allow for a wide variety of applications under different conditions. This study aims to form the basis for a reliable and more realistic prediction of the CLT members supported by soil and obtain more accurate simulations of CLT samples by modeling and analyzing the failure modes of wood, adhesives and soil. Some of the great applications of wood composites include high and low-rise residential and non-residential buildings, temporary bridges and access mats in mine discoveries and oil and gas industry. The proposed research has the potential to broaden these applications of wood by making use of its favorable properties that will lead to safer and more energy efficient structural systems, and better industrial applications. In summary, this research has been performed in order to achieve the following objectives:

1. Achieve better understanding of Cross Laminated Timber mat structures, material properties, unique orientation and the advantages of their applications
2. Develop a nonlinear finite element analysis procedure capable of predicting the behavior of CLT and the main occurring failure modes
3. Validate the FEA results against experimental results previously performed
4. Study the effect of the adhesives between the CLT mats and the significance in modeling
5. Perform a comparison between traditional wood mats and CLT mats

6. Study and identify the parameters needed to model soil nonlinearly
7. Investigate the effect of placing CLT members in soil
8. Study the CLT and Soil failure modes and investigate which one experience failure first
9. Based on existing literature, propose modifications to current industrial practices published guides by highlighting their limitations and propose recommendations on how to design CLT mats

CHAPTER 2: MODELING

2.1 Prior Experimental Work

Recent experimental work has been done by Mahamid et al (Behavior & Strength Characteristics of Cross Laminated Timber Mats: Experimental and Numerical Study,2017) [2]. In this paper, the authors performed experimental work of CLT Members in bending and shear; they tested 20 specimens in bending and 20 in shear to obtain the reference bending and shear design values, F_b and F_v respectively, of CLT members with unique arrangements of Southern Yellow Pine (SYP) No. 2 grade, using 2x8 nominal dimensional members. CLT Assemblies tested and their dimensions are presented in the table below (Table 1).

Table 1: CLT Assemblies Dimensions tested in laboratory

Test Assembly Designation	CLT Assembly Thickness (in.)	CLT Assembly Width (in.)	CLT Assembly Length (in.)	Distance between Supports (in.)
B1	6.831	15.037	216	204
B2	6.821	15.091	216	204
C1	6.741	15.113	216	204
C2	7.041	14.912	216	204
Average Values	6.85	15	216	204

The average values of the dimensions were calculated to model the representative 5-ply CLT specimen with a thickness of 6.85 inches (total of 5 layers with 1.37-inch thickness of each layer), width of 15 inches, total length of 216 inches and distance between supports of 206 inches. Figure 2(a) and 2(b) show the sketch of the simply supported beam under pure bending test as well as the geometry of the CLT specimen. Three-Dimensional finite element models were created for the

same CLT arrangements tested experimentally by Mahamid et al (2017) [2] using the finite element software (ANSYS 17.1 and 18.1). Results obtained by the finite element were compared to experimental results for validation.

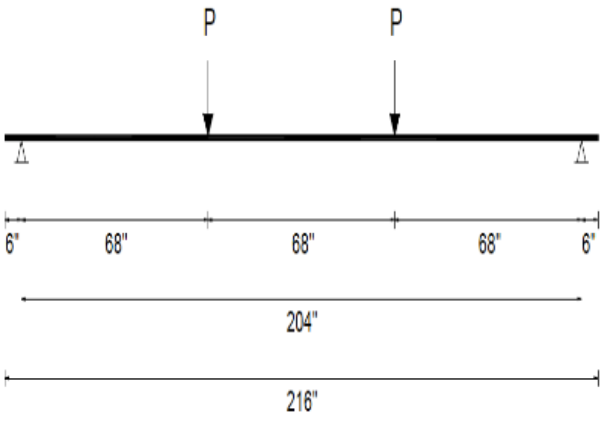

Figure 2: (a) Sketch of the beam, loading and supports

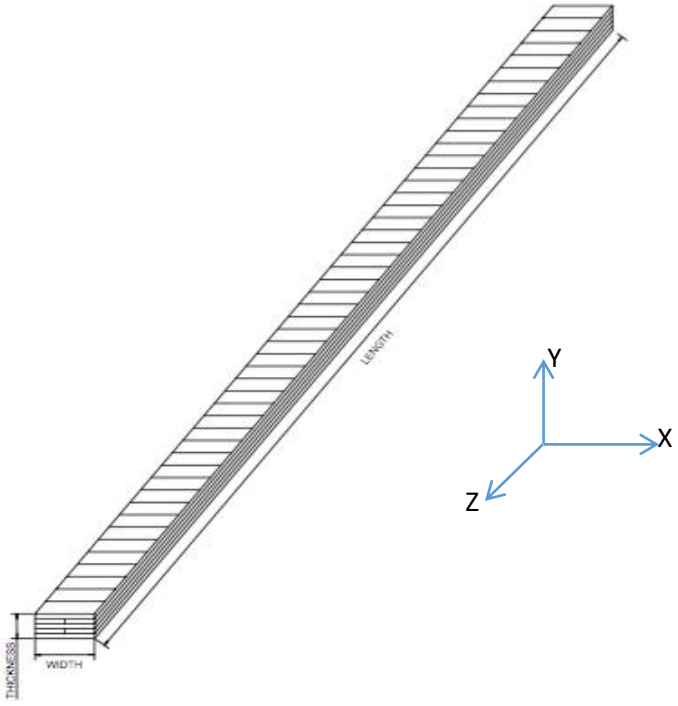

Figure 2: (b) CLT specimen

2.2. Model Characteristics

The CLT layers are modeled using SOLID186 element type in ANSYS which is commonly used for 3D modeling of structures and is a higher order 3-D 20-node solid element that exhibits quadratic displacement behavior. The element is defined by 20 nodes having three degrees of freedom per node: translations in the nodal x, y, and z directions. The element supports plasticity, hyperelasticity, creep, stress stiffening, large deflection, and large strain capabilities [4].

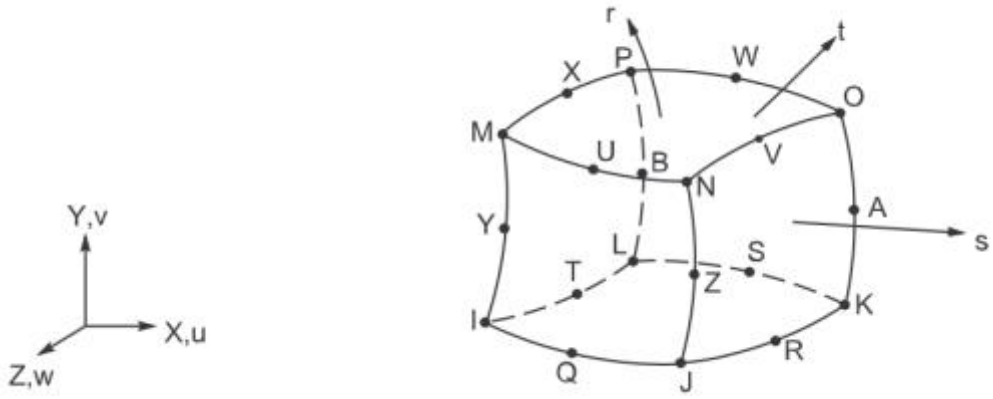

Figure 3: SOLID186 Structural Solid Element

Other elements are target elements and contact elements to simulate the behavior between the different layers of CLT assembly and interface between soil and wood. Target elements (TARGE170) are used to represent 3-D "target" surfaces for the associated contact elements (Figure 4). 3-D 8- Node Surface-to-Surface contact element (CONTA174) are used to represent contact and sliding between 3-d target surfaces and a deformable surface defined by this element(Figure 5). CONTA174 element has the same geometric characteristics as the solid or shell element face with which it is connected [34]. Contact occurs when the element surface penetrates an associated target face. Figure 4 and 5 [34] represent the geometry of the target and contact elements used in modeling respectively.

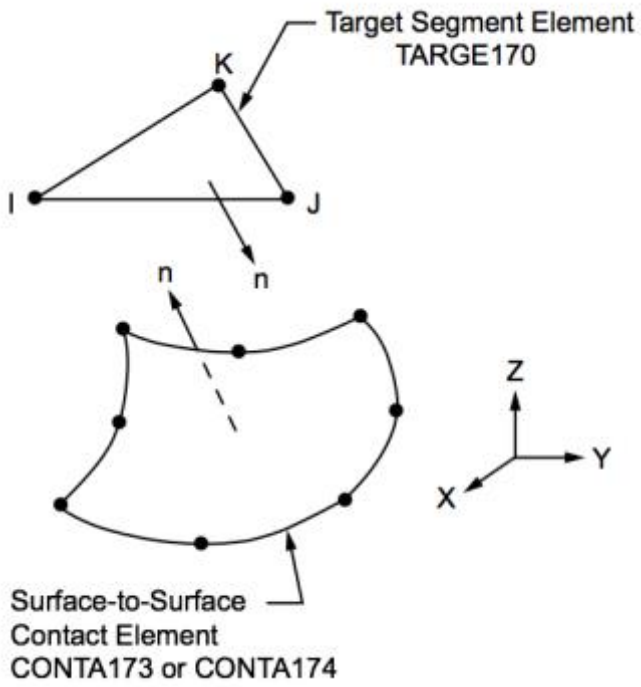

Figure 4: TARGE170 Element Geometry

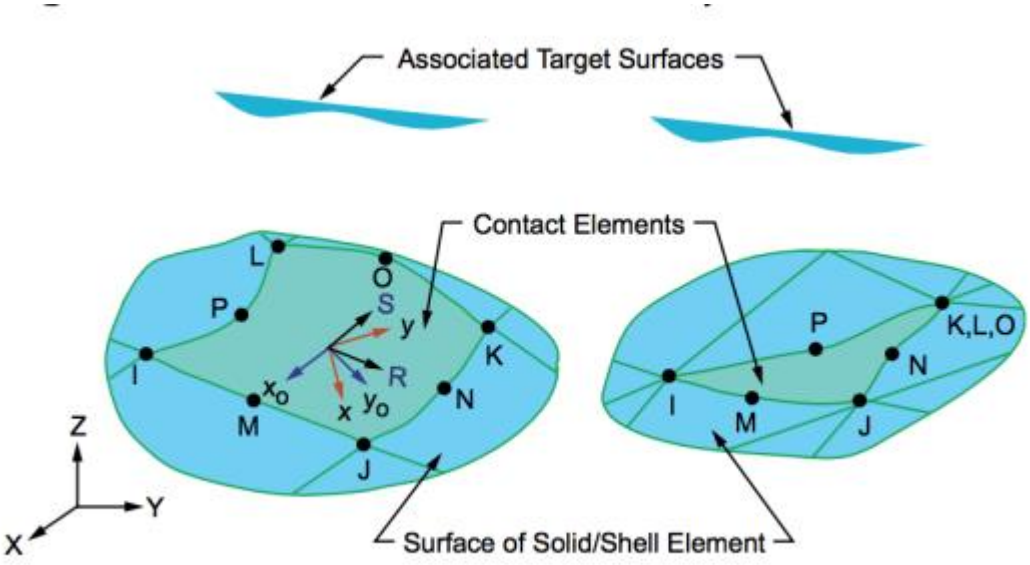

Figure 5: CONTA174 Element Geometry

Bonded contact elements are used between CLT layers to allow the surfaces to be in perfect contact with each other throughout the analysis and the loads to be transmitted from one part to the adjacent part. Frictional contact with a 0.2 frictional coefficient was used to simulate the behavior between wood and soil as well between vertical joints above the neutral axis of CLT. Frictionless contact was used to simulate the behavior between vertical joints below the neutral axis. Frictional contact represents the realistic behavior between CLT and soil by allowing CLT to slide on the target surface of soil in the tangential direction. The difference between bonded and frictional contact is that bonded contact does not simulate a gap that allows the contact to open and close and does not allow sliding whereas the frictional contact simulates the contact to open and close as well as allows sliding if $F_{sliding}$ (force caused by sliding) is greater than $F_{friction}$ (force caused by friction defined by the friction coefficient). Frictionless contact allows the gap to open and close and allows sliding with a friction coefficient of 0 [4]. The element orientation is another important property of CLT because the layers of wood are placed in orthogonally alternating orientation to the neighboring layers as shown in Figure 8. The boundary conditions were assigned as simply supported beam, similar to the experiment by restraining the displacement on all directions on one edge and restraining the displacement on x and y-axis but allowing it to freely move in the z-axis on the other edge. Two equal line pressures were applied based on the sketch from Figure 2(a) at a constant distance between supports (204 in) as shown in Figure 5. Figure 6 represents the meshed finite element model and Figure 7 shows the loading under 4-point pure bending test and boundary conditions.

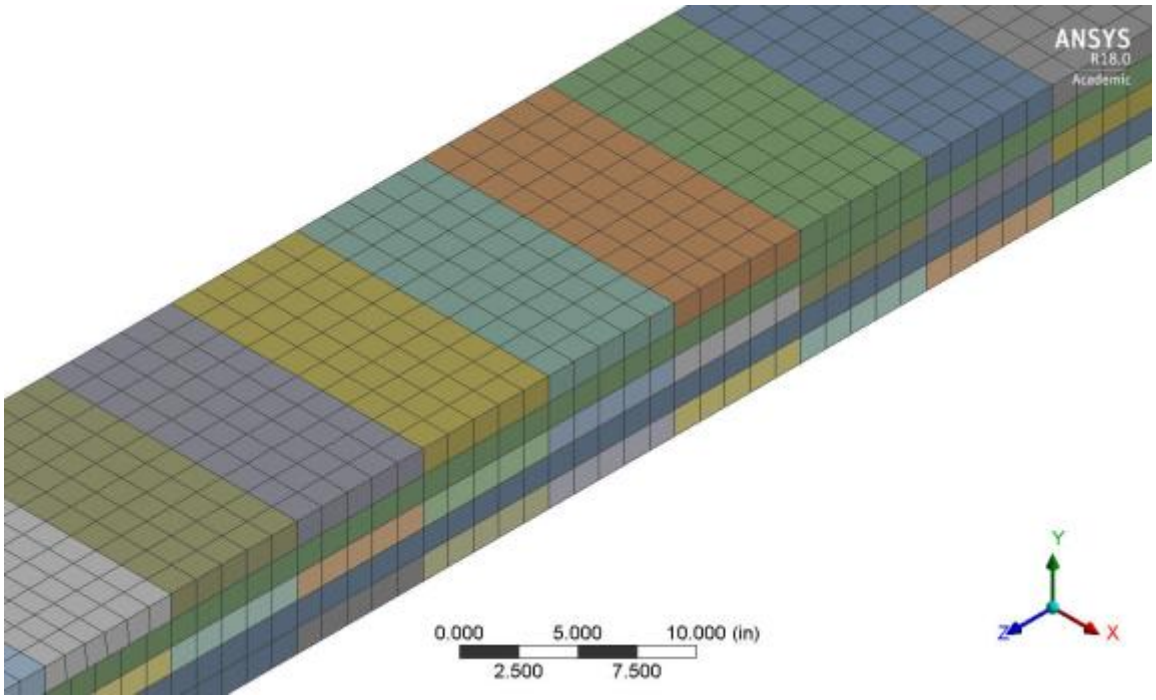

Figure 6: Meshed Model

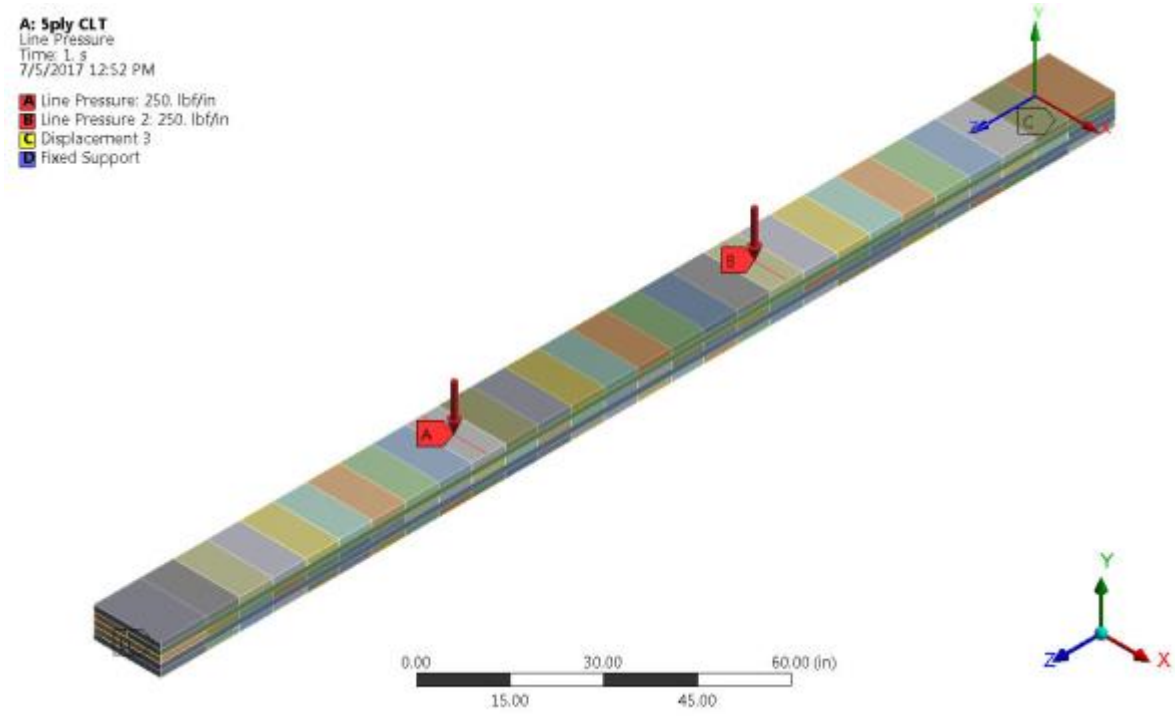

Figure 7: Loading for Bending Test

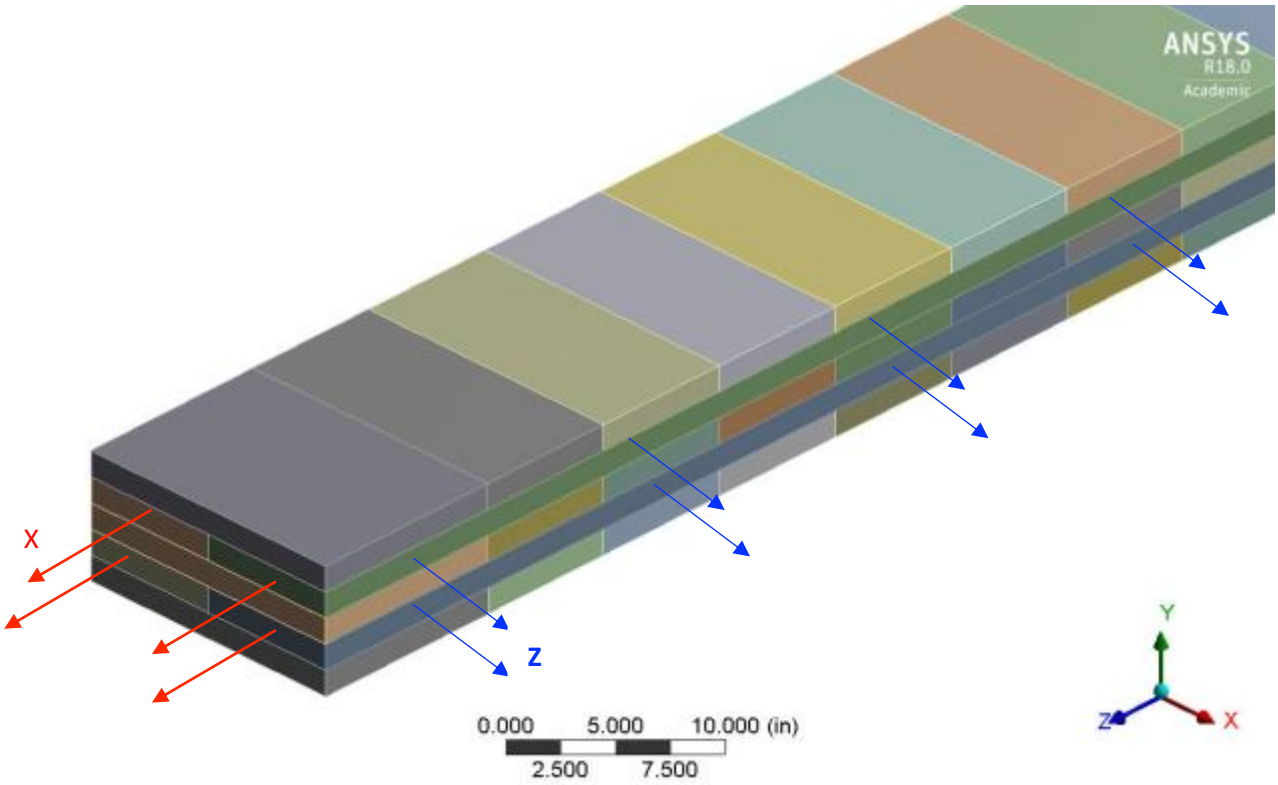

Figure 8: Element Orientation of CLT

2.3. Material Properties and Modeling of Wood using ANSYS

2.3.1. Orthotropic Elastic Material Properties

Wood is defined as an orthotropic material, which means that it has different material properties in all 3 defined coordinate axes: longitudinal, transversal and radial. Orthotropic Elasticity is used to model wood in the elastic region. The following material properties sown in Table 2 were obtained from the tension test performed at the Forest Product Laboratory in Madison, WI by Mahamid et al. (2017) [2] and from the relationships of properties obtained from the Wood Handbook [3].

Table 2: Orthotropic Linear Elastic Material Properties of wood

Orthotropic Elasticity	Value	Unit
Young Modulus X direction	1,600,000	psi
Young Modulus Y direction	180,800	psi
Young Modulus Z direction	124,800	psi
Poisson Ratio XY	0.382	
Poisson Ratio YZ	0.292	
Poisson Ratio XZ	0.362	
Shear Modulus XY	131,200	psi
Shear Modulus YZ	20,800	psi
Shear Modulus XZ	129,600	psi

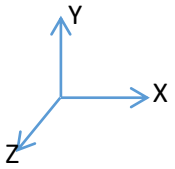

2.3.2. Damage Model of Wood

One of the main methods to study the behavior of composites in ANSYS is progressive damage, which represents the damaged behavior of the model as the load is increased. Once the stress reaches the damage limit, the material stiffness is instantly reduced to a user-specified value [8]. This technique requires the definition of linear elastic-orthotropic material properties and three material models explained below:

-Damage Initiation Criteria

-Damage Evolution Law

-Material Strength Limits

Damage Initiation defines the criterion type for determining the start of the material damage. Criteria include: maximum strain, maximum stress, Puck, Hashin, and LaRc 03/LaRc04.

Maximum Stress criterion identifies composite material failure caused by three possible modes of loading (longitudinal failure, transverse failure, and shear failure) for tensile fiber, compressive fiber, tensile matrix and compressive matrix [9]. This criterion considers that the composite section fails when the stress exceeds the respective allowable stresses based on these parameters. Maximum Strain criterion identifies composite material failure caused by three possible modes of loading (longitudinal failure, transverse failure, and shear failure) for tensile fiber, compressive fiber, tensile matrix and compressive matrix [9]. This criterion considers that the composite section fails when the strain exceeds the respective allowable strain values based on these parameters. Hashin criterion takes into account interactions between stresses and strains on a lamina and identifies two failure modes: fiber failure and matrix failure, distinguishing between tension and compression. Puck criterion identifies fiber and inter-fiber failure in a unidirectional composite. In this criterion, the composite material type and the selected fiber properties need to be specified [9].

LaRc03 (2-D) and LaRc04 (3-D) are two sets of failure criteria for laminated-fiber reinforced composites, which are based on physical models for each failure mode and distinguish between fiber and matrix failure for different transverse fiber and matrix tension and compression modes. LaRc04 assumes linear shear behavior and small angle deflection [9]. The criterion chosen for this model is "Maximum Stress" criterion, due to available stress limits of CLT obtained from previous experiments (Mahamid et al. [2]). All possible failure modes of this criterion are defined in equations 1 through 4 based on the following parameters [9]:

S_{11}^{+}=Value of σ_{11} at longitudinal tensile failure

S_{11}^{-}= Value of σ_{11} at longitudinal compressive failure

S_{22}^{+}=Value of σ_{22} at transverse tensile failure

S_{22}^{-}=Value of σ_{22} at transverse compressive failure

S_{12}= Absolute value of σ_{12} at longitudinal shear failure

Longitudinal failure occurs whenever

$$\sigma_{11} \geq S_{11}^{+} \text{ or } \sigma_{11} \leq S_{11}^{-} \quad (1)$$

Transverse failure occurs whenever

$$\sigma_{22} \geq S_{22}^{+} \text{ or } \sigma_{22} \leq S_{22}^{-} \quad (2)$$

Longitudinal shear failure occurs whenever

$$|\sigma_{12}| \geq \sigma_{12}^{max} \quad (3)$$

Failure Index = Max. Absolute value of

$$\left(\frac{\sigma_{11}}{S_{11}^{+}}, \frac{\sigma_{11}}{S_{11}^{-}}, \frac{\sigma_{22}}{S_{22}^{+}}, \frac{\sigma_{22}}{s_{22}^{-}}, \frac{\sigma_{12}}{s_{12}^{-}}\right) \geq 1 \quad (4)$$

Since the failure index is a simple ratio of stresses, the failure load can be computed by simply dividing the applied load by the failure index.

Damage Evolution Law defines how the material degrades after the damage has occurred. This law models the rate of instant stiffness reduction by defining user inputs for tensile and compressive stiffness in the fibers and in the matrix [8]. The values that represent the level of

damage can range from 0 (no damage) to 1 (complete damage). This model uses a calibrated value of 0.25, which was calibrated with experimental results, as the instant reduction factors for bending models. Material Strength Limits are the maximum stresses that a material can withstand before damage is observed. Table 3 shows the orthotropic limits of the CLT specimen.

Table 3: Orthotropic Stress Limits of wood

Orthotropic Stress Limits	Value	Unit
Tensile X direction	2,789	Psi
Tensile Y direction	470	Psi
Tensile Z direction	470	Psi
Compression X direction	-3,940	Psi
Compression Y direction	-790	Psi
Compression Z direction	-790	Psi
Shear XY/YZ/XZ	1,300	Psi

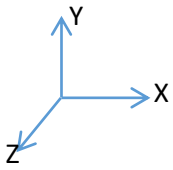

2.4. Material Properties and Modeling of Soil using ANSYS

Soil is considered a complex material to analyze using finite element analysis due to the complicated material properties and non-uniformity and gradation of the material. Soft soil is used to support CLT members and observe the failure modes in both wood and soil. Soft soil properties used to reflect the use of timber for such applications in the real-world applications which is timber mats that are used when the soil is not stiff enough. The material model used in ANSYS is Isotropic Elastic using Young's Modulus (E) and Poisson's Ratio (μ). To model non-linearity in soil, Drucker Prager Model was used. This material model describes pressure-dependent inelastic materials and uses the outer cone approximation to the Mohr-Coulomb law to determine if a

material has failed or undergone plastic yielding [10]. The input data consists of the Drucker Prager Base and Failure Plan Data Set. The Drucker Prager Base has three input values: uniaxial compressive strength, uniaxial tensile strength and biaxial compressive strength.

Uniaxial compressive strength of soils is the unconfined compressive strength of soils, which represents the behavior and gradation of soils. In this case the loading is unidirectional, perpendicular to the failure plane, whereas the biaxial compressive strength is obtained by applying loading in two different directions. For the type of soil pertaining to this study, the uniaxial compressive strength is the dominant characteristic compared to biaxial compressive strength. However, in order to allow the data set to be compatible, the biaxial compressive strength needs to be at least a value higher than the uniaxial compressive strength defined and cannot be neglected. The tensile strength of soils is very low and mostly negligible.

The Failure plane data consist of the following parameters:

-Inner Frictional Angle (φ)

-Initial Cohesion (c)

-Dilatancy Angle (ψ)

-Residual Internal Friction Angle

-Residual Cohesion

The angle of internal friction is defined as the ability of soil to withstand shear forces applied to the soil. It is the angle (φ), measured between the normal force (N) and resultant force (R), that is attained when failure just occurs in response to a shear stress (S). Its tangent (S/N) is the coefficient of sliding friction [11]. Its value is determined experimentally and is constant for different types of soil. The initial cohesion value is the force that holds together molecules within the soil and is determined by the Direct Shear Test. Cohesive soils are usually the clay type of soil. The dilatancy angle is dependent on the internal friction angle and controls an amount of plastic volumetric strain

(change in volume) during plastic shearing and is assumed constant during plastic yielding. In other words, it represents the increase in material volume due to yielding. In FEA and numerical methods, an associated plastic flow rule is assumed which means that the angle of dilation is assumed to be equal to the angle of internal friction [16]. If the residual strength parameters (residual cohesion and residua internal angle of friction) are equal to the peak values of cohesion and angle of internal friction, this defines an elastic perfectly plastic material. If residual strength parameters are assigned as 0, this defines a brittle material [33]. Figure 9 represents the Drucker Prager yield function [13].

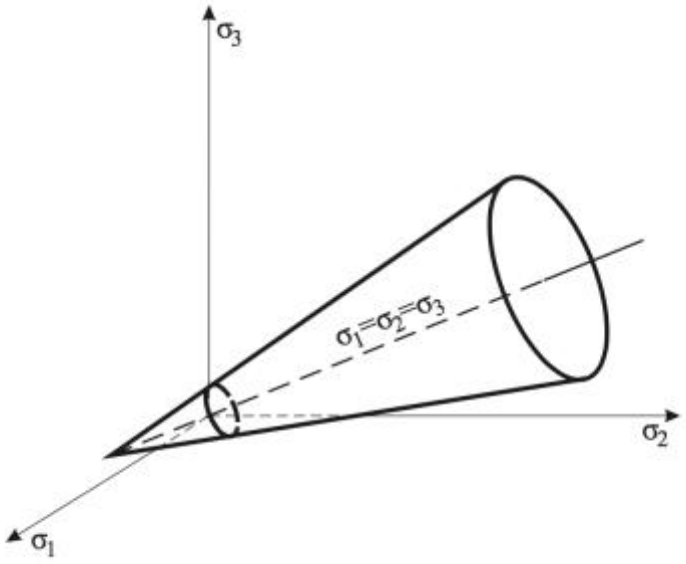

Figure 9: Drucker-Prager Yield surface in principal stress space

In the principal stress space (σ_1, σ_2 , σ_3), this surface represents a cone. The yield surface equation of this model is shown in Equation 5 [13].

$$f=\alpha I_1 + \sqrt{J_{2D}} - k \qquad (5)$$

If non-associated yield condition is defined, the plastic potential surface is defined following Equation 6 [13].

$$g = \beta I_1 + \sqrt{J_{2D}} \qquad (6)$$

where:

I_1 is the first stress invariant, J_{2D} represents second stress deviatoric invariant and terms α, β and k represent arbitrary parameters of the material model, which can be calculated using parameters of the Mohr-Coulomb model [14].

Most of the material properties were obtained from extensive literature search and previous experimental work performed to define soft soils, which is of interest for the purpose of this study. Elastic and inelastic properties of clays are presented in Table 4 [11], [15], [33].

Table 4: Elastic and Inelastic Soil Material Properties

Elastic Properties	Value	Unit
Young's Modulus	1421.37	psi
Poisson's Ratio	0.3	
Non-Elastic Properties	Value	Unit
Uniaxial Compressive Strength	3.47-13.89	psi
Inner Friction Angle	24	degrees
Cohesion Value	870.22	psi
Dilatancy Angle	24	degrees
Residual Cohesion Value	145.04	psi
Residual Inner Friction Angle	20	degrees

2.5. Material Properties and Modeling of Glue using ANSYS

CLT panels consist of multiple layers of lumber boards stacked orthogonally crosswise and glued together on their common faces [1]. The glue is another material used to predict the overall behavior of CLT, which is complicated in modeling due to its material properties. Surface elements of 0.05-inch thickness were used to model each layer of adhesive. SHELL181 element is used to model thin shell structures and represents a four-node element with six degrees of freedom at each node: translations in the x, y, and z directions, and rotations about the x, y, and z-axes [4]. The type of adhesives in CLT shall meet the same requirements as the ones used in glued laminated timber, which include qualified polyurethane, melamine and phenolics. The material properties were obtained from the material data sheet of Generic Polyurethane (PUR) [18]. The material model used for the glue is isotropic elastic and in order to model nonlinearity, bilinear isotropic hardening model was used. After testing the glue in the CLT model up to failure, it was concluded that wood fails prior to glue. Due to the insignificant thickness of glue and since glue does not experience failure before wood, bonded contact between the wood layers can be used to replace the modeling of adhesives and represent the bond behavior in CLT mats. Table 5 represents elastic and inelastic material properties of CLT Adhesives [17] , [18], [19].

Table 5: CLT Adhesives Material Properties

Elastic/Non-Elastic Properties	Value	Unit
Young's Modulus	282100	Psi
Poisson's Ratio	0.38	
Yield Strength	4206	Psi
Tangent Modulus	8020	Psi

CHAPTER 3: MODEL VERIFICATIONS

To validate the Finite Element (FE) models used in this study, the results obtained were compared with the experimental results from Mahamid et al. (2017) [2].

3.1 Load Displacement Curves

The finite element results were verified by comparing them with Mahamid et al. (2017) [2], load-deflection curves for the same configuration obtained from FEM (Figure 6 and 7) and experimental results. As can be observed from the curves in Figure 10, there is a very good agreement between the FEA and experimental data. The overall percentage error of FEA data compared to experimental results of tested members B1, C1, B2 and C2 (Table 1) was calculated to be 9.87% which falls within acceptable ranges. The FEA curve represents a good average curve or best fit line to all the experimental data.

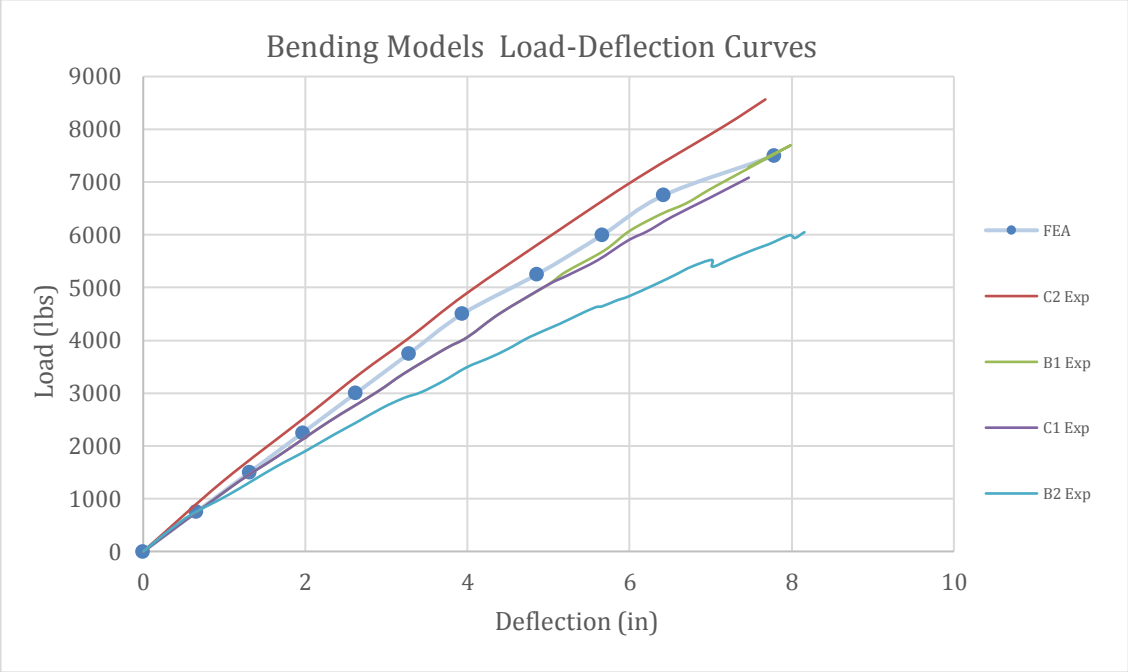

Figure 10: Load-Deflection Curve (Experimental vs FEA Model)

3.2. Deflections, Stresses and Damage Status of the CLT Model

The deflection results of the beam in pure bending are shown in Figure 11. Bending stresses, damage status and shear stresses of wood are shown in Figures 12, 13 and 14 respectively. Under two equal applied line pressures of 250 lbf/in each, leading to a total force of 7500 lbs, the deformation at midspan is 7.78 inches as shown in figure 11. The highest shear stress that wood experiences is about 104 psi as shown in figure 13 and the highest bending stress about the z axis that occurs is 4710 psi as shown in figure 12. As expected due to the pure bending test, there is no shear between the loads in the middle third of the support. The damage is mostly observed in the second and fourth layer of wood as shown in Figure 13 because of the unique orientation of layers of CLT (Figure 8). The damage in wood occurred in bending and not in shear due to the normal stresses exceeding the stress limits in tension and compression as defined in the failure damage model (4710 psi > 2789 psi and 4564 psi > 3940 psi).

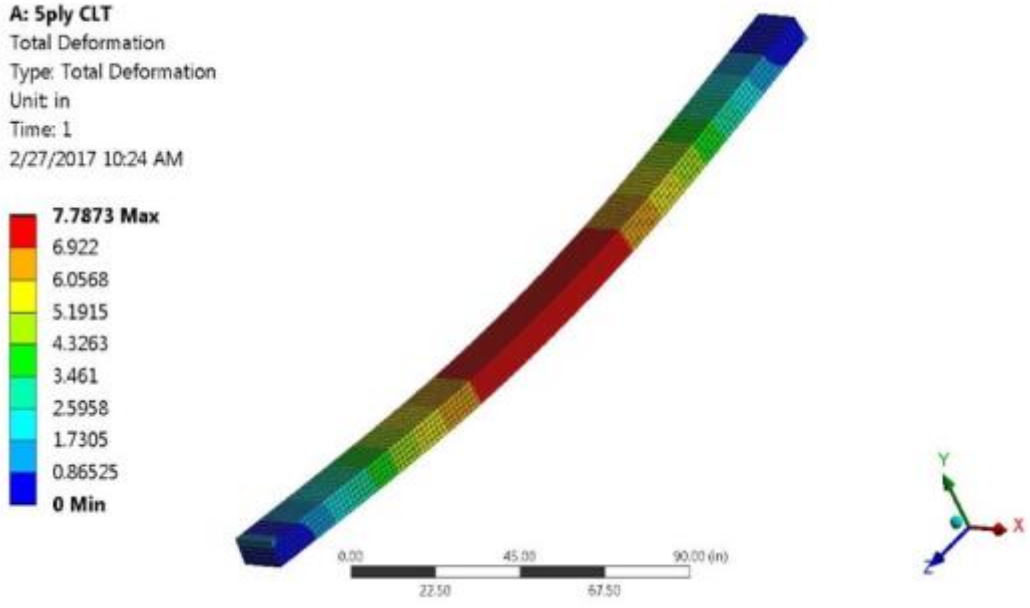

Figure 11: Deflection Results

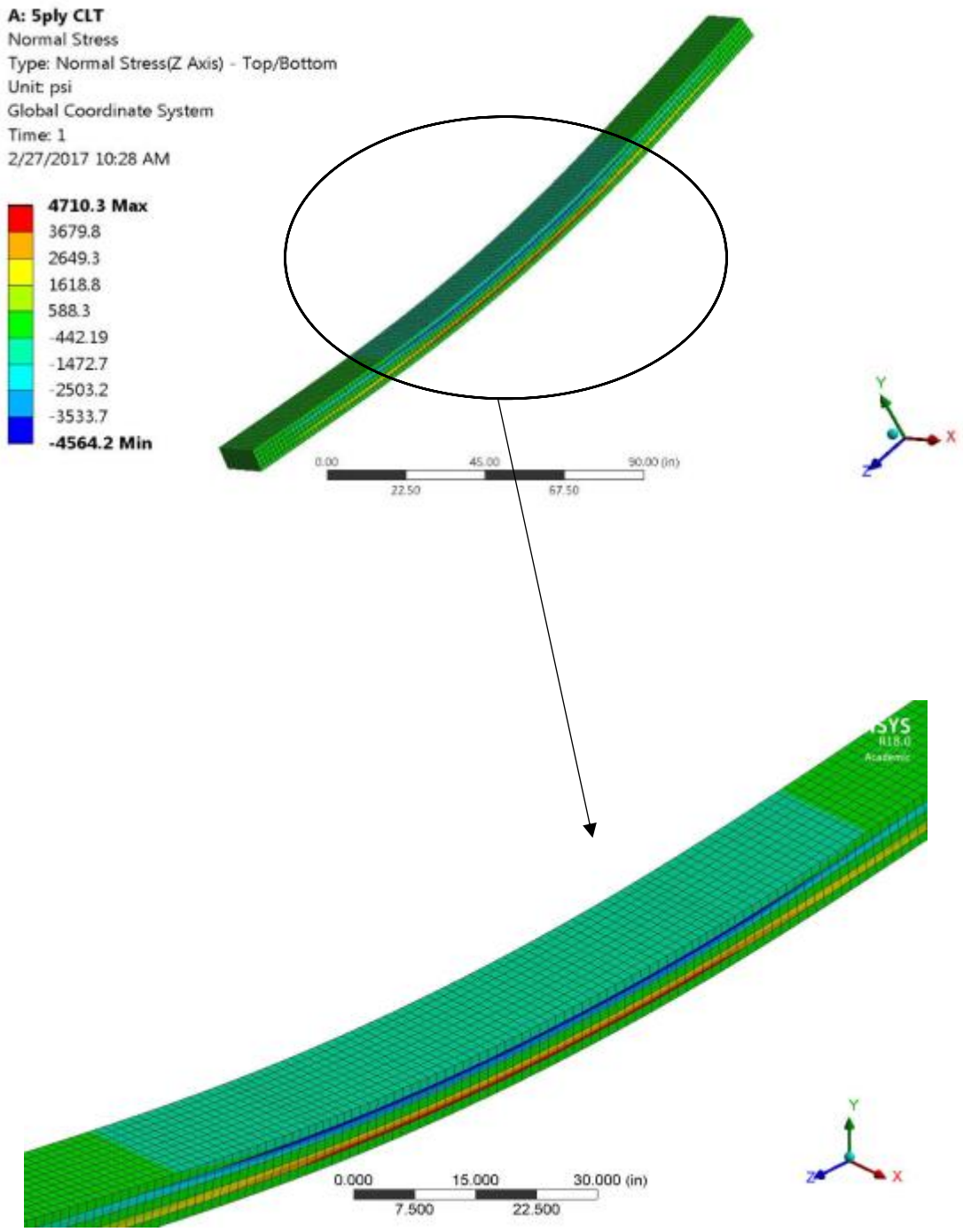

Figure 12: Normal Stresses (z-axis)

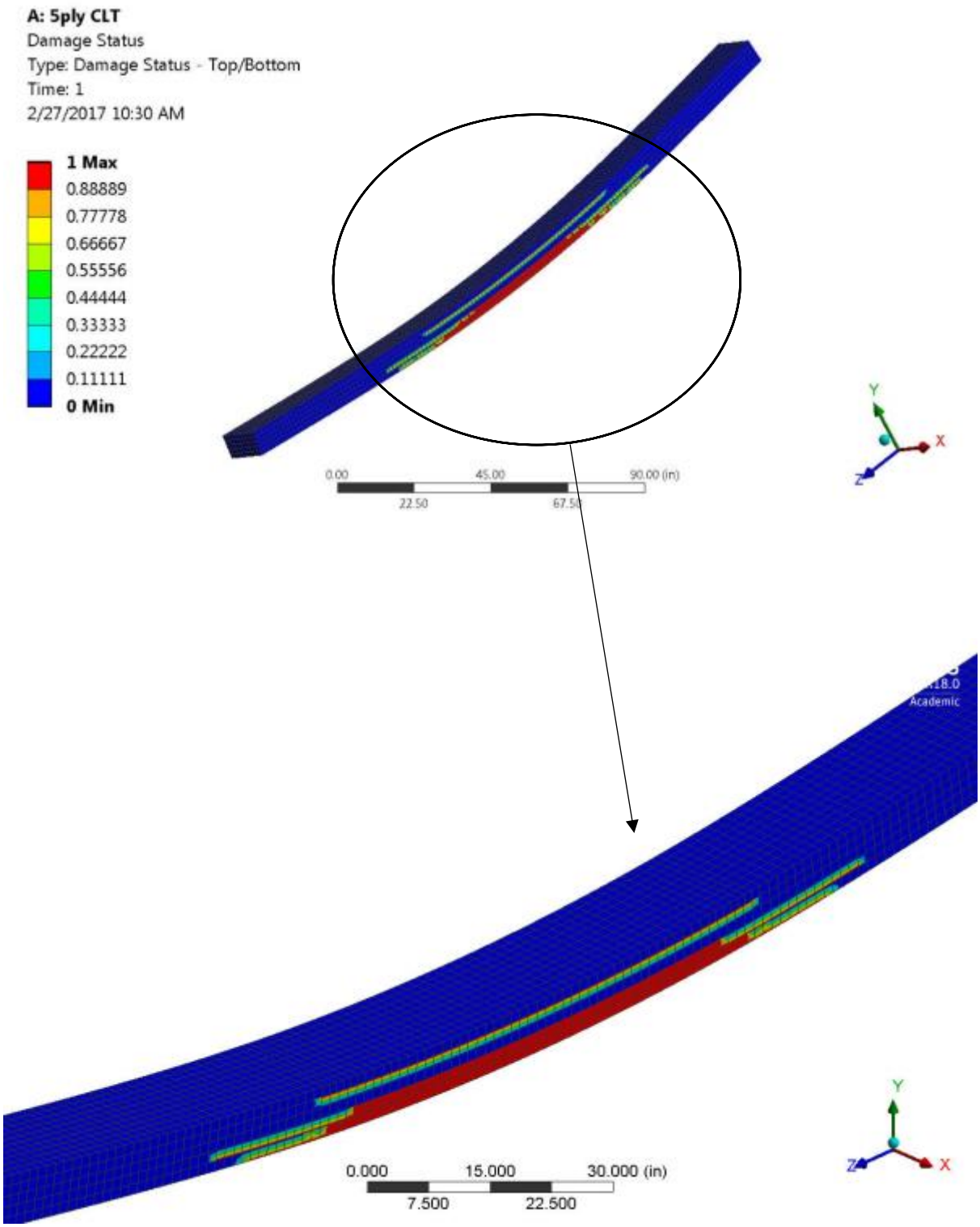

Figure 13: Damage Status

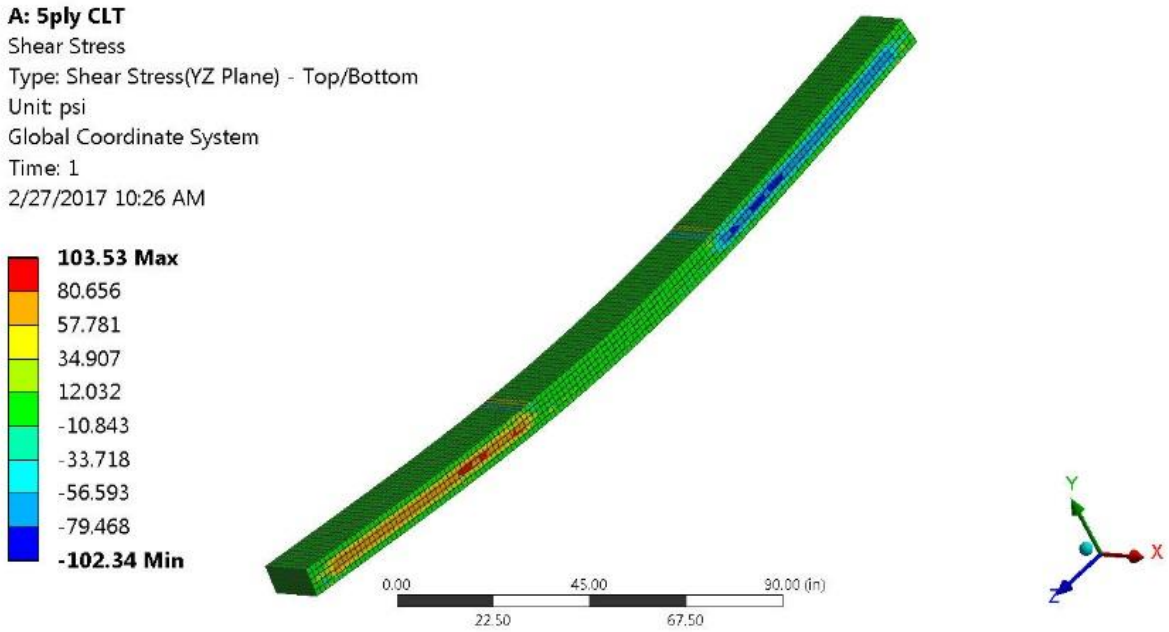

Figure 14: Shear Stresses (YZ Plane)

In conclusion, the proposed FEA procedure is a powerful tool to simulate the behavior of CLT mats. The FEA allowed to capture the primary failure modes of the experiments and showed reliable results compared to experimental results. Thus, this model can be used to investigate timber mats behavior supported by the soil.

CHAPTER 4: COMPARISON BETWEEN CLT AND TRADITIONAL MATS

A comparison was carried out between the behavior of wood traditional mats composed of heavy timber members and steel rods and different configurations of CLT mats. A comparison was performed between 5-ply and 7-ply CLT mats and a 12 in. thick traditional wood members connected by 4 1-in. diameter A36 steel rods placed along the length of wood. All models are made out of Southern Yellow Pine (SYP) No.2 grade and simply supported boundary conditions were provided at the bottom far ends of the members. This comparison highlights the advantages of using CLT in this application.

4.1. 5-layer CLT mat

Southern Yellow Pine No.2 CLT member with the following parameters and conditions was built and analyzed.

-Total span of 185 in. (Figure 15)

-Total thickness of 6.875 in. (1.375 in. per layer) (Figure 15)

-Simply supported at the bottom far ends of the member (Figure 15)

-Pressure applied as two equal line pressures at each third of its span (Figure 17)

-Typical unique orientation of layers of CLT (Figure 8)

Figure 15 shows the geometry of the 5-ply CLT mat. Figure 16 and 17 show the mesh and the loading pattern respectively. A total pressure of 30,000 lbs. was applied and the analysis results were recorded and analyzed (Figure 18-21).

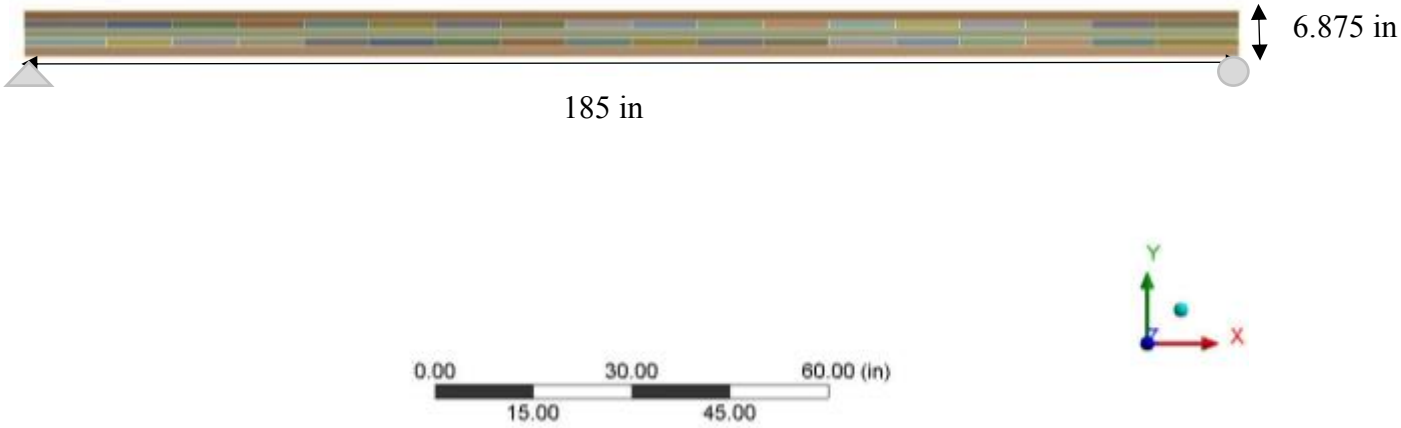

Figure 15: Geometry of 5-ply CLT

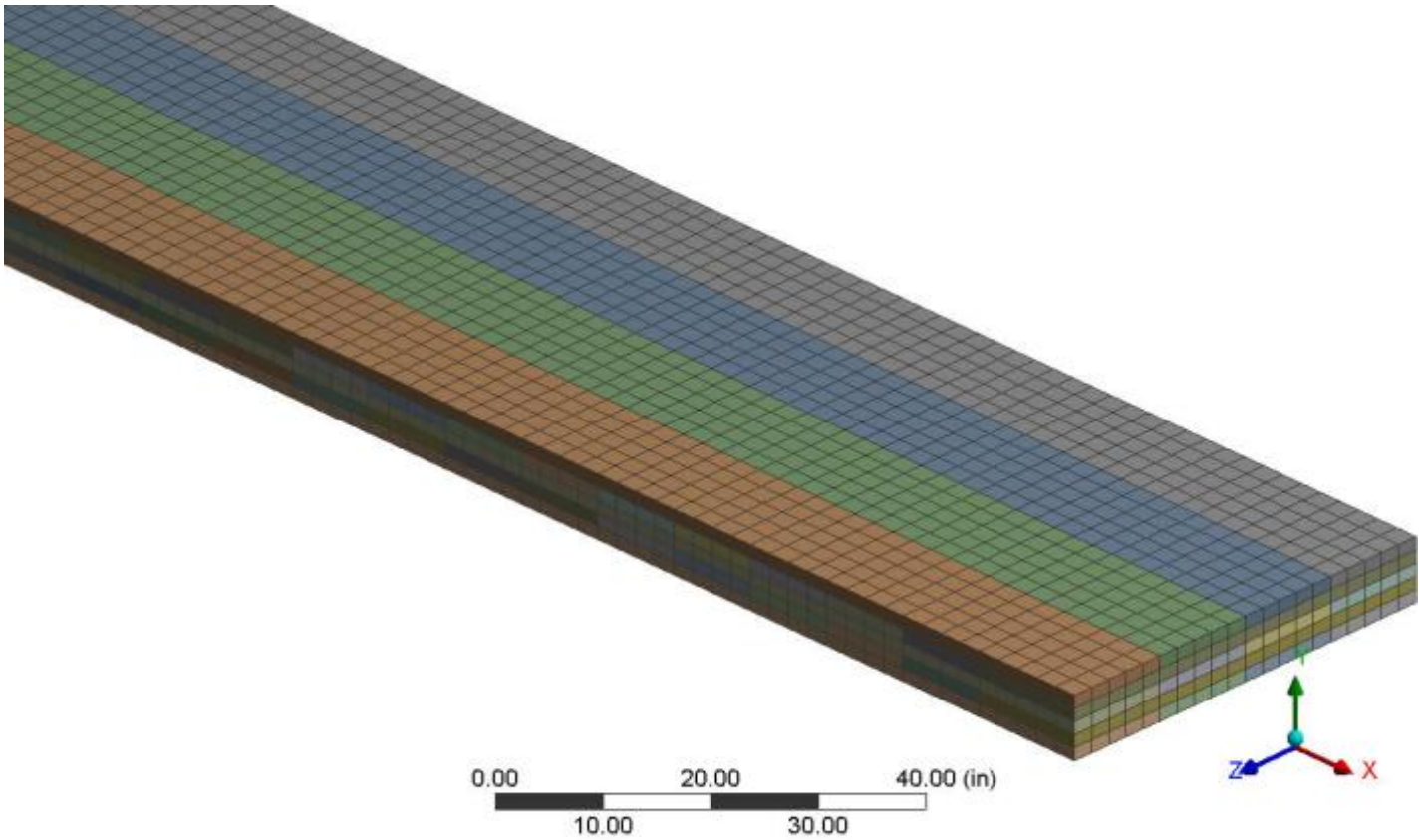

Figure 16: Meshed model

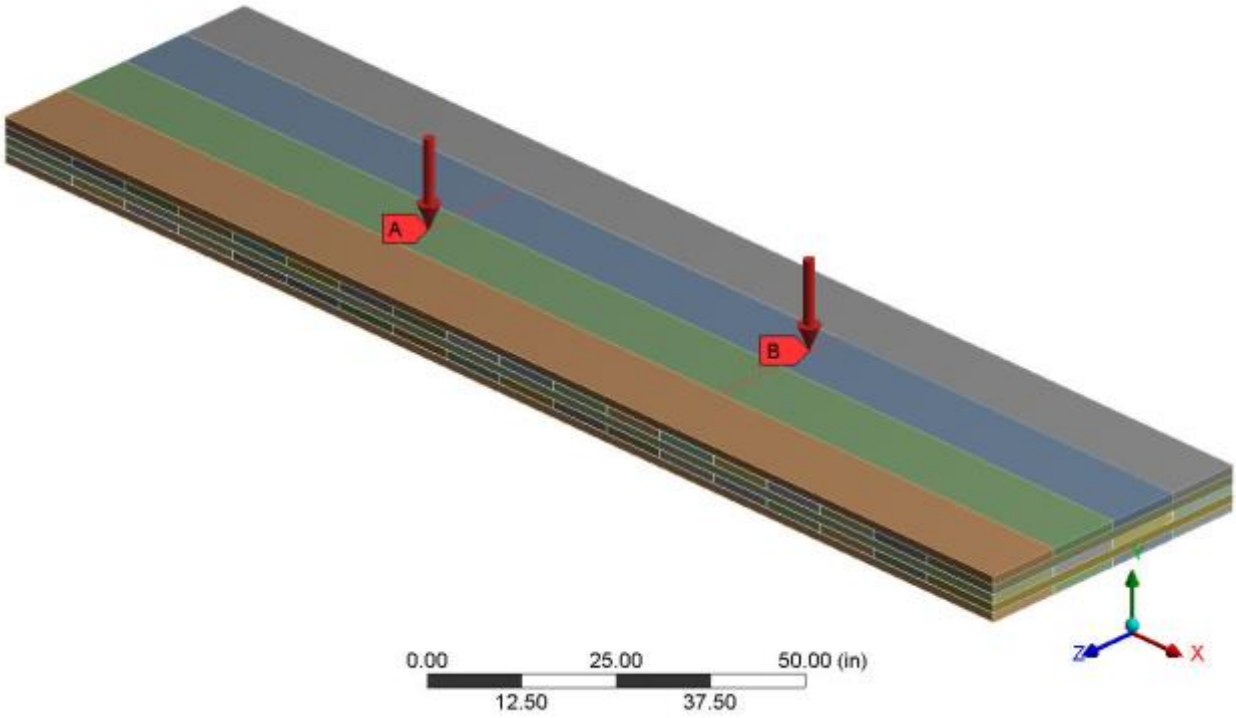

Figure 17: Loading

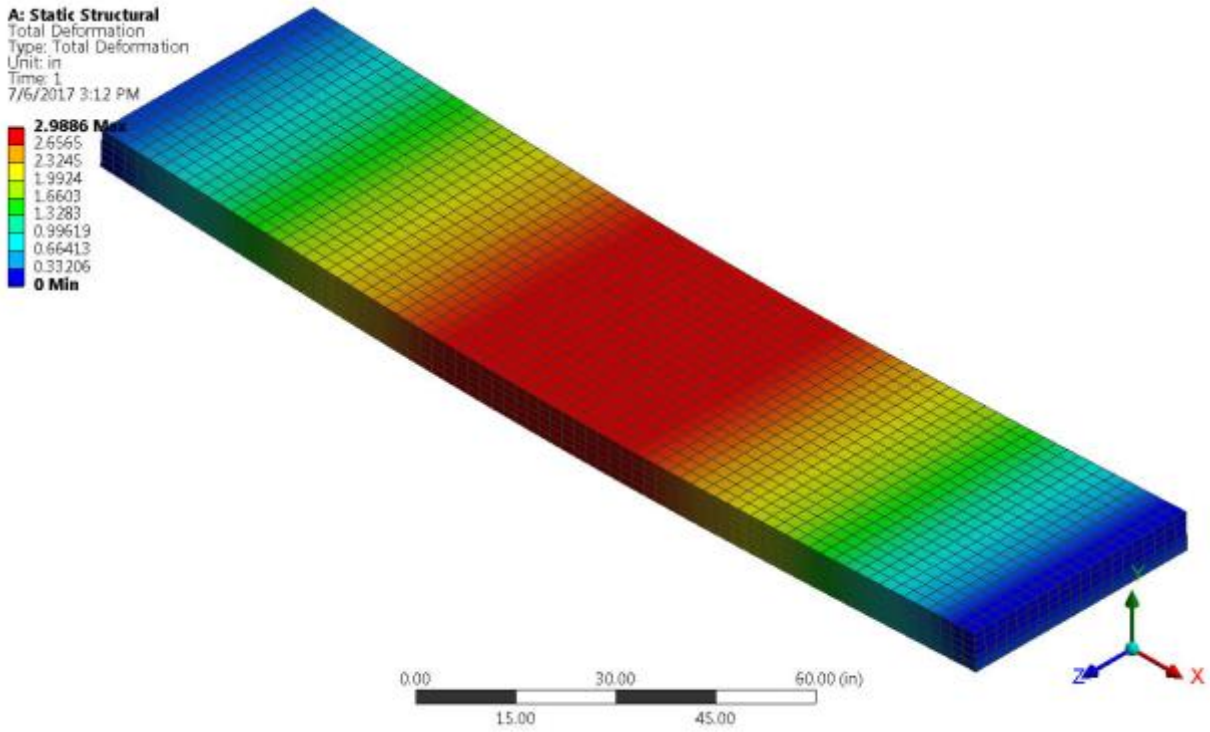

Figure 18: Deflection Results

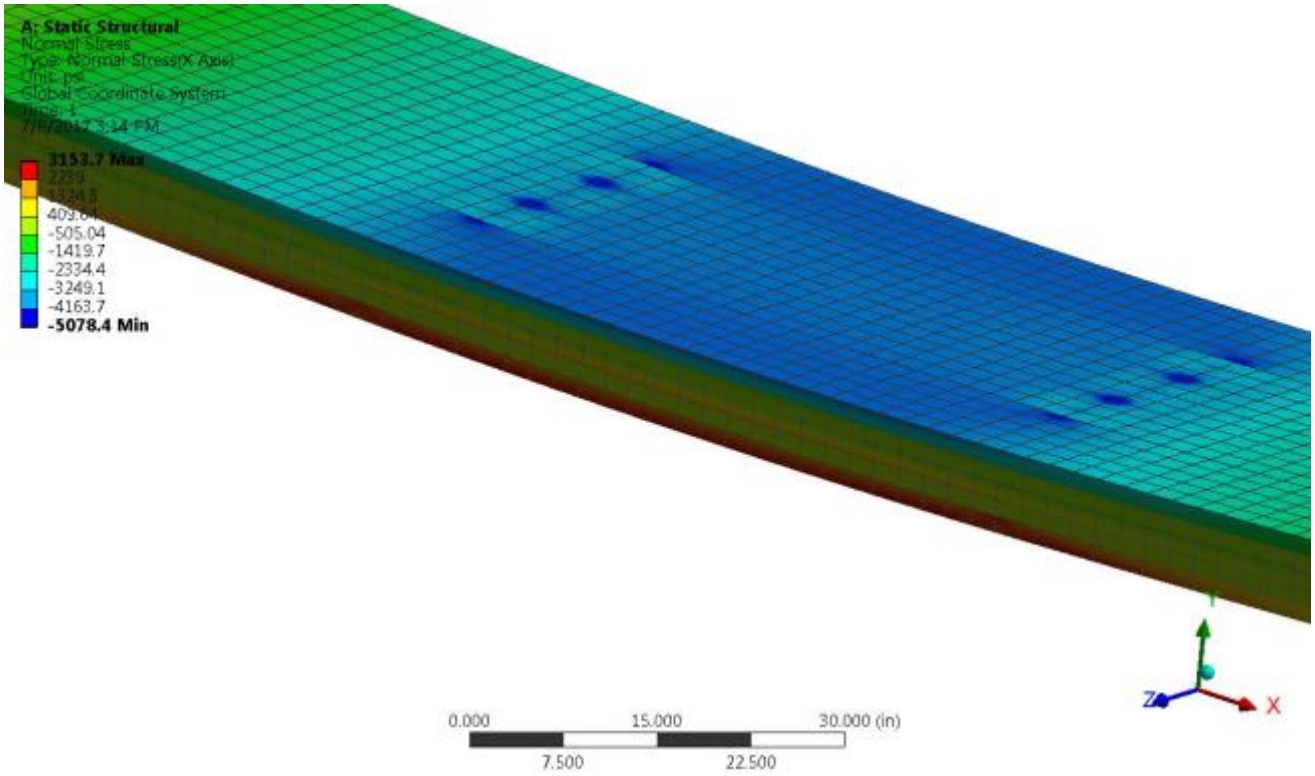

Figure 19: Normal Stresses (x-axis)

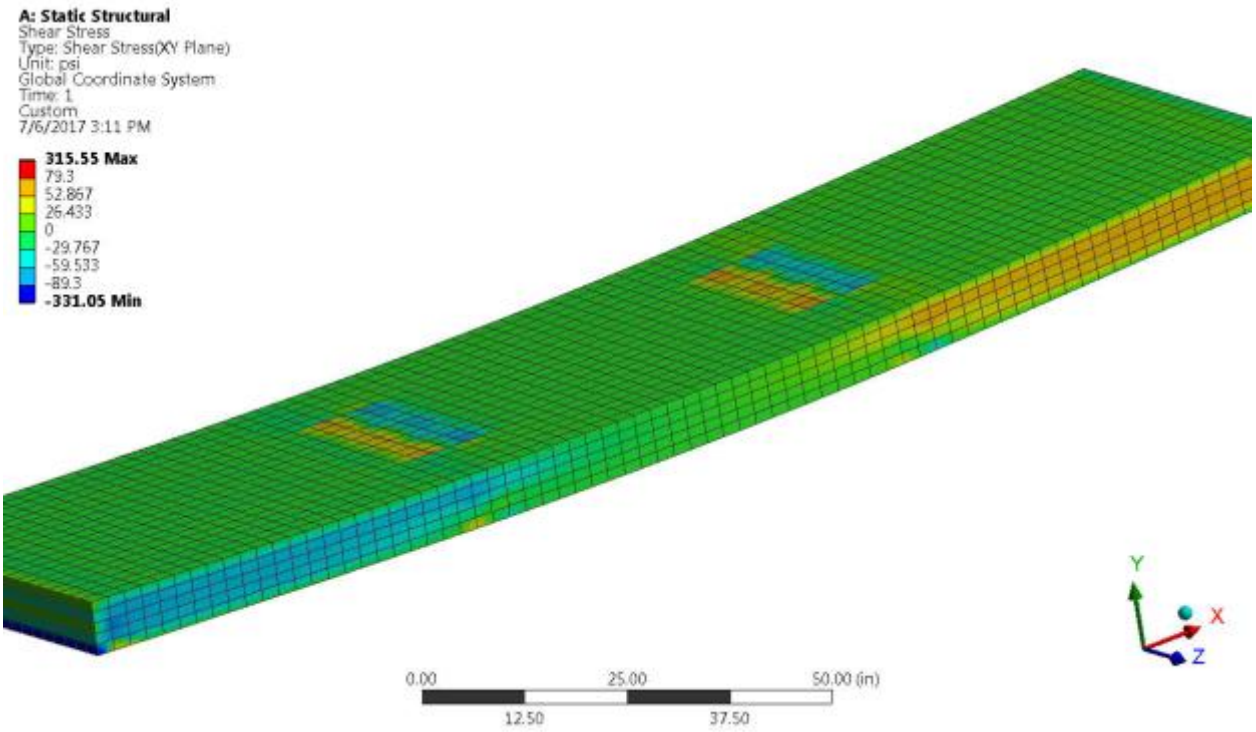

Figure 20: Shear Stresses (XY Plane)

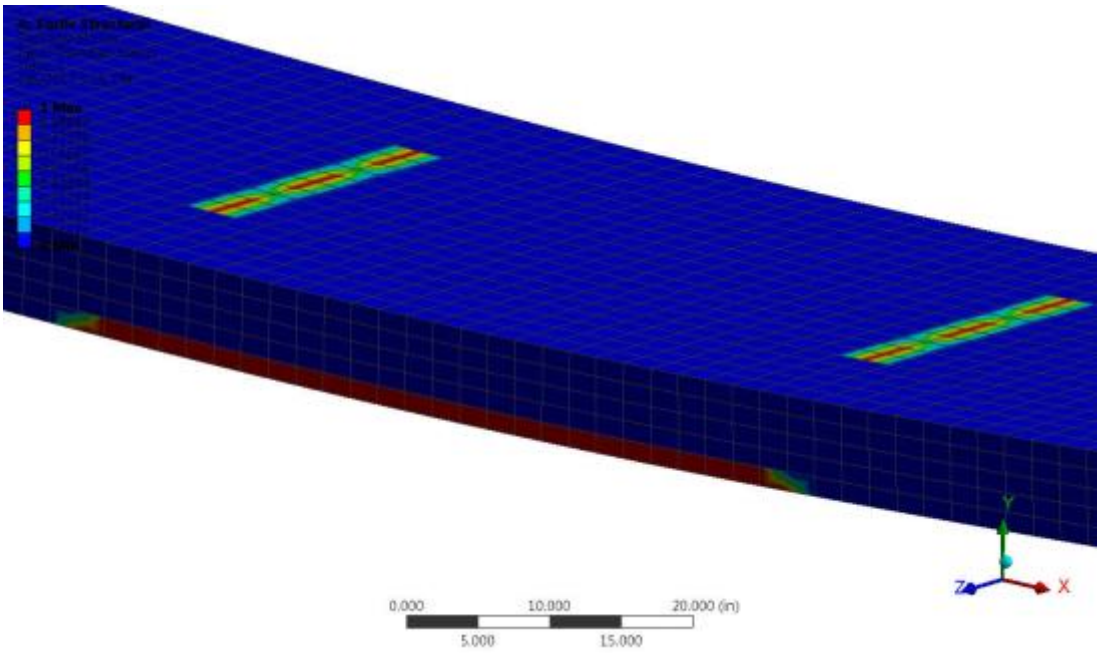

Figure 21: Damage Status

Under the given loading, the maximum deformation recorded is 2.98 inches (Figure 18), the maximum bending stresses about the major axis (x-axis) are 3152.7 psi in tension and -5078.3 psi in compression (Figure 19). The top layer of the member is in tension and the bottom layer is in compression. The highest shear stresses the mat experiences about the XY plane are 79.8 psi and -89.3 psi (Figure 20). There is no shear stresses at the middle third of the span since the member is in pure bending. Due to the stress limits being exceeded in bending (3152.7 psi > 2789 psi and 5978.3 psi > 3940 psi), damage occurs around the location of the applied line pressures at the top as well as in the middle third of the span at the bottom layer. The damage is obvious at the bottom layer since that layer is fully in tension and bending stresses have been exceeded. The analysis results of the 5 ply CLT mat are summarized in Table 6.

Table 6: 5-layer CLT mat Analysis Results

Total Load Applied		Results
30 000 lbs.	Deformation (in)	2.98
	Damage	Yes
	Normal Stresses (psi)	3153.7
		-5078.3
	Shear Stresses (psi)	79.8
		-89.3

4.2. 7-layer CLT mat

Southern Yellow Pine No.2 CLT member with the following parameters and conditions was built and analyzed.

-Total span of 185 in (Figure 22)

-Total thickness of 9.625 in. (1.375 in. per layer) (Figure 22)

-Simply supported at the bottom far ends of the member (Figure 22)

-Pressure applied as two equal line pressures at each third of its span (Same load pattern as Figure 17)

-Typical unique orientation of layers of CLT (Figure 8)

Figure 22 shows the geometry of the 7-ply CLT mat and Figure 23 shows the meshed model. Similar to the loading pattern applied to the 5-ply CLT (Figure 17), a total pressure of 45000 lbs. was applied and the analysis results were recorded and analyzed (Figure 24-27)

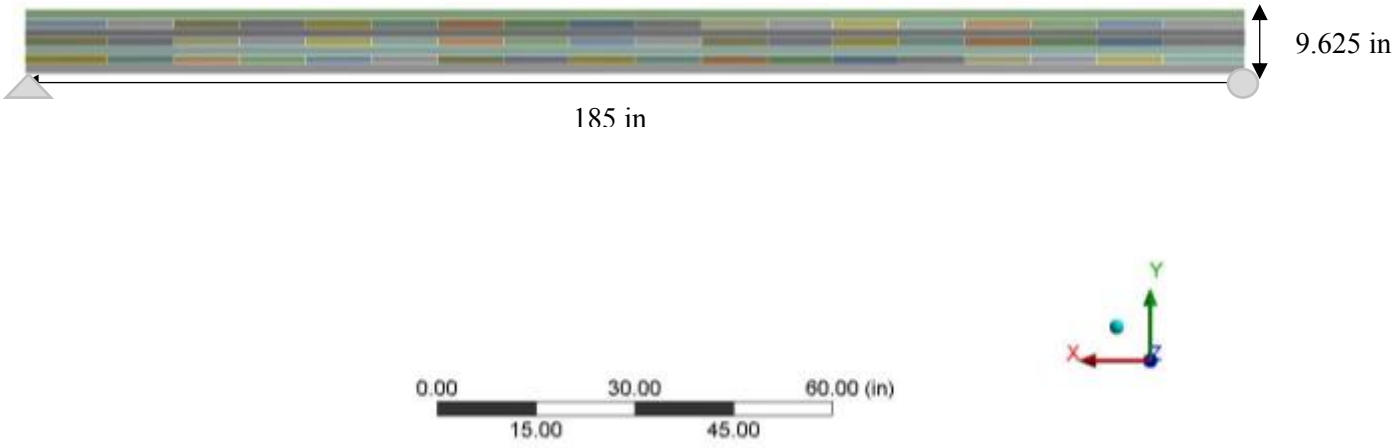

Figure 22: Geometry of 7-ply CLT

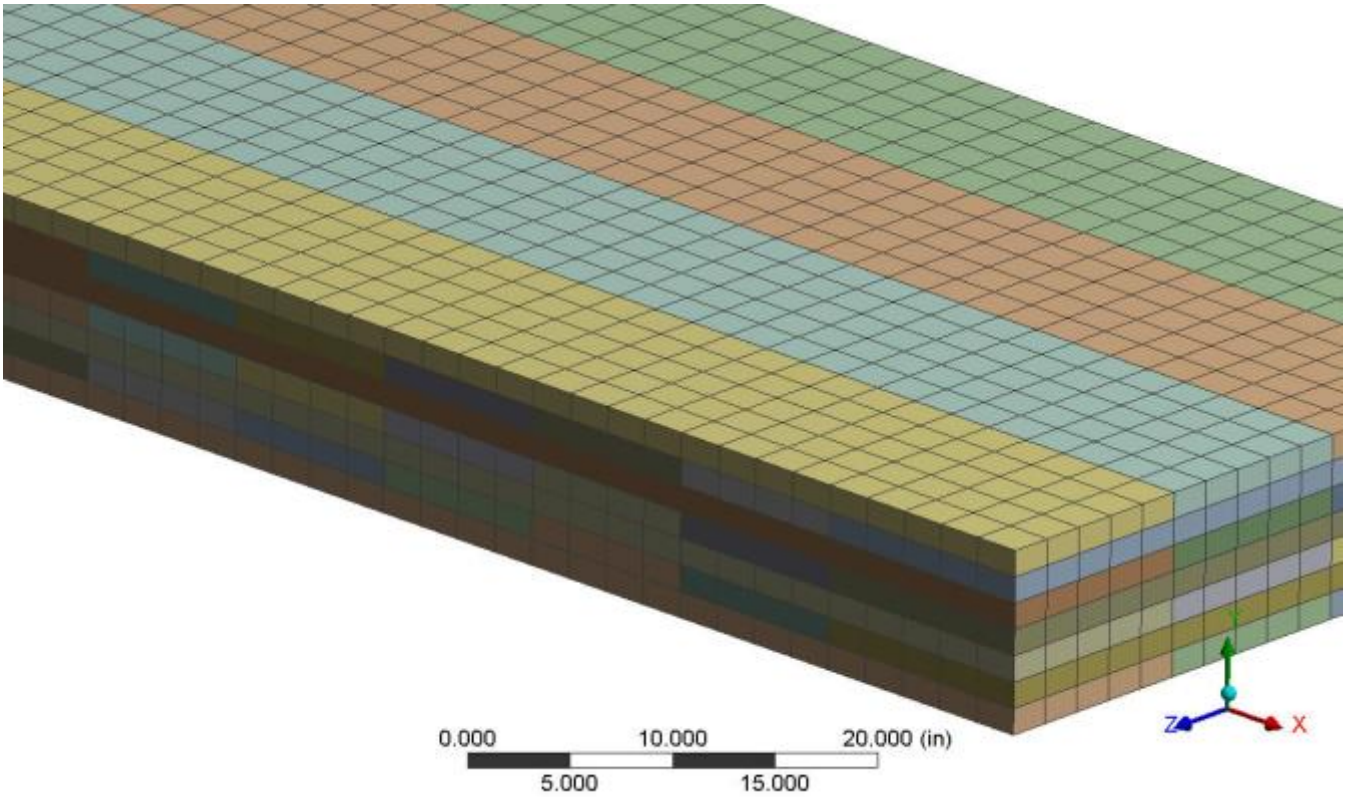

Figure 23: Meshed Model

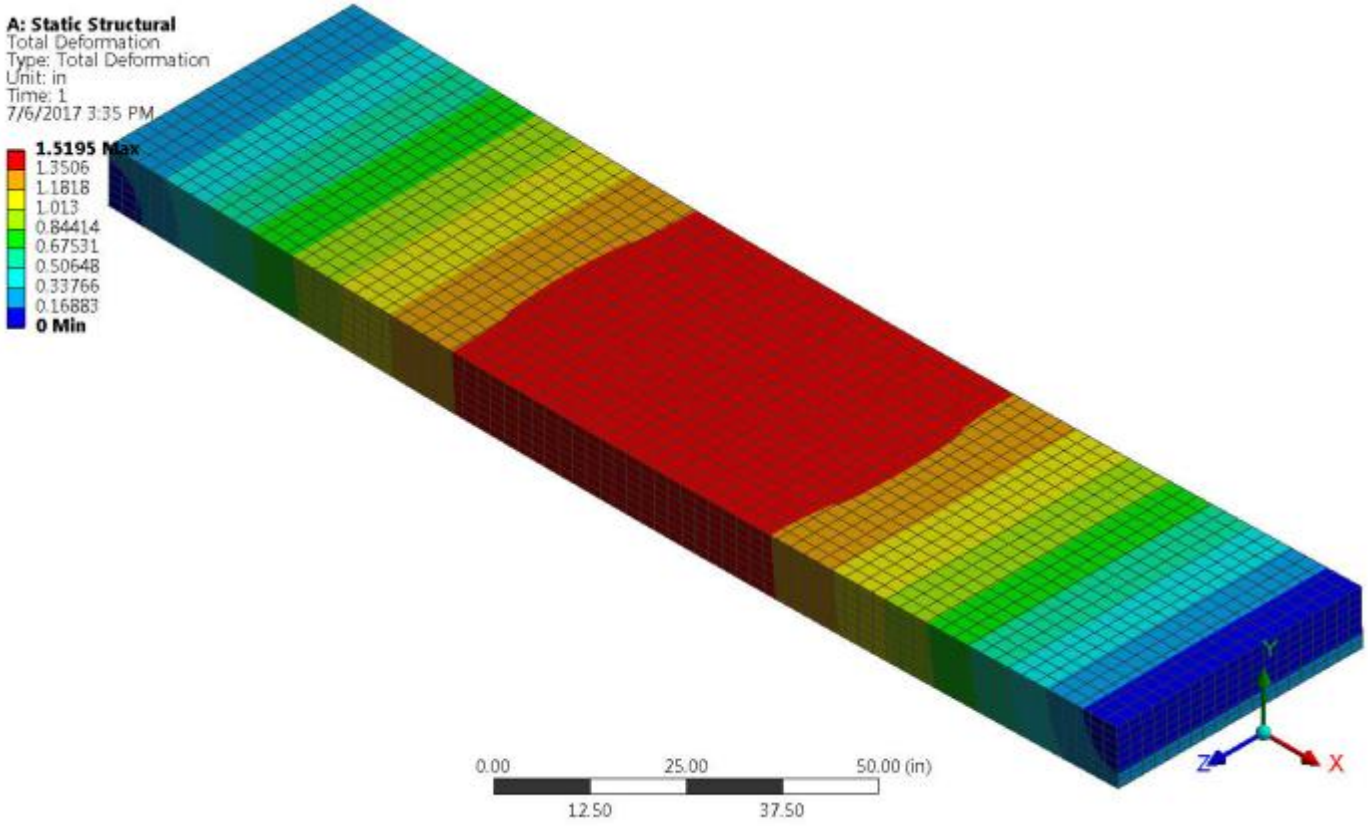

Figure 24: Deflection Results

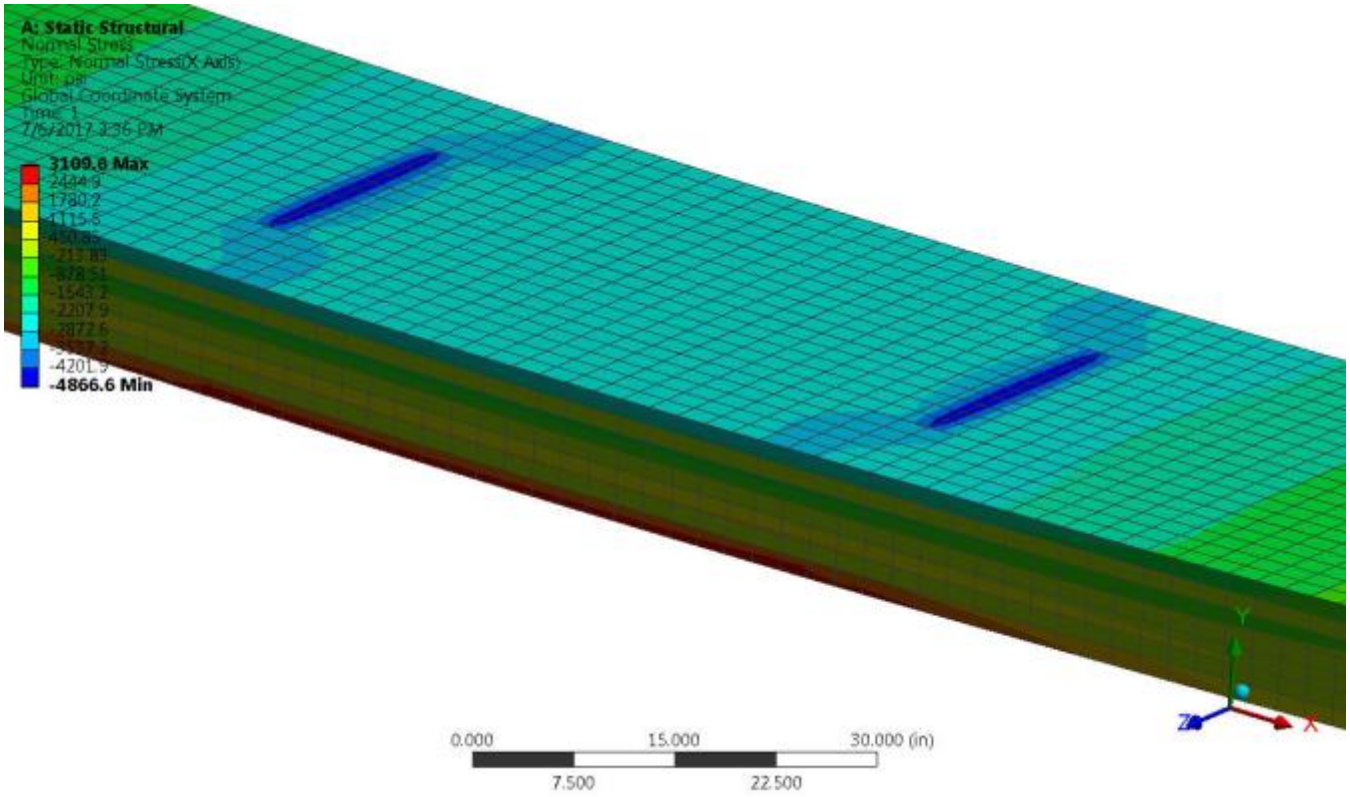

Figure 25: Normal Stresses (x-axis)

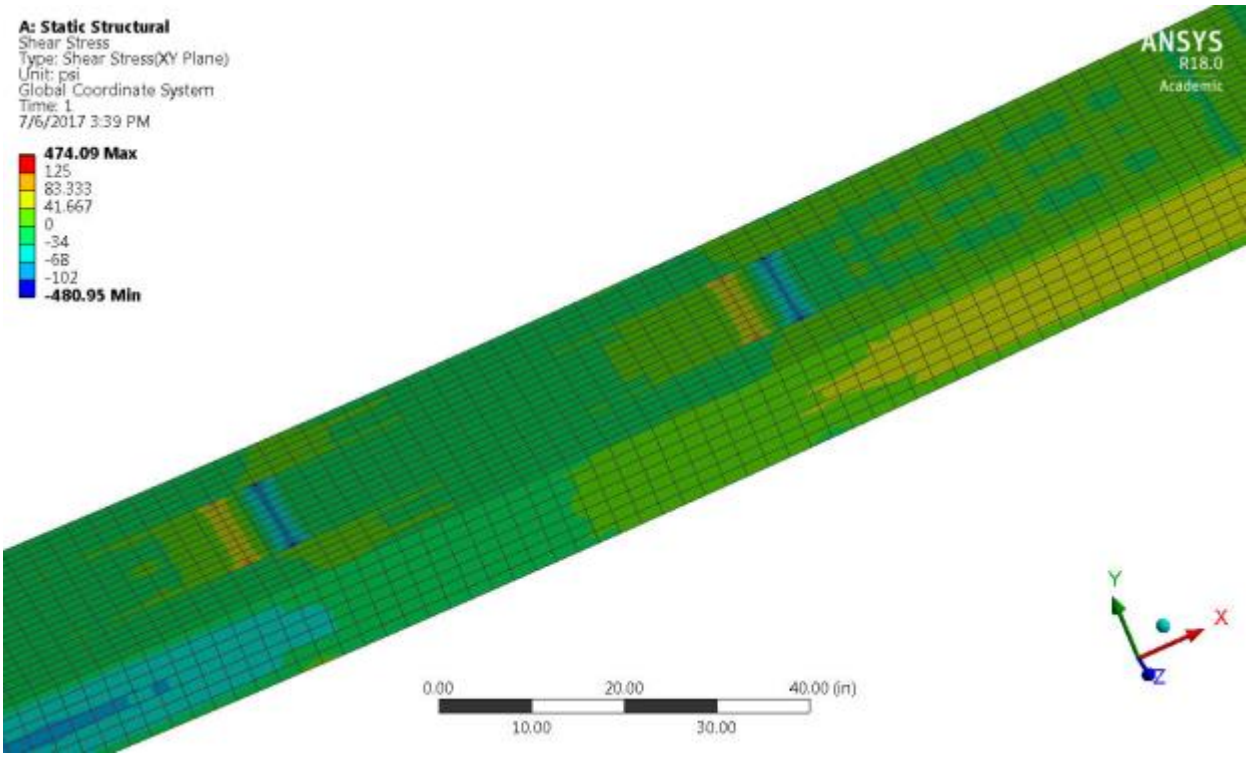

Figure 26: Shear Stresses (XY Plane)

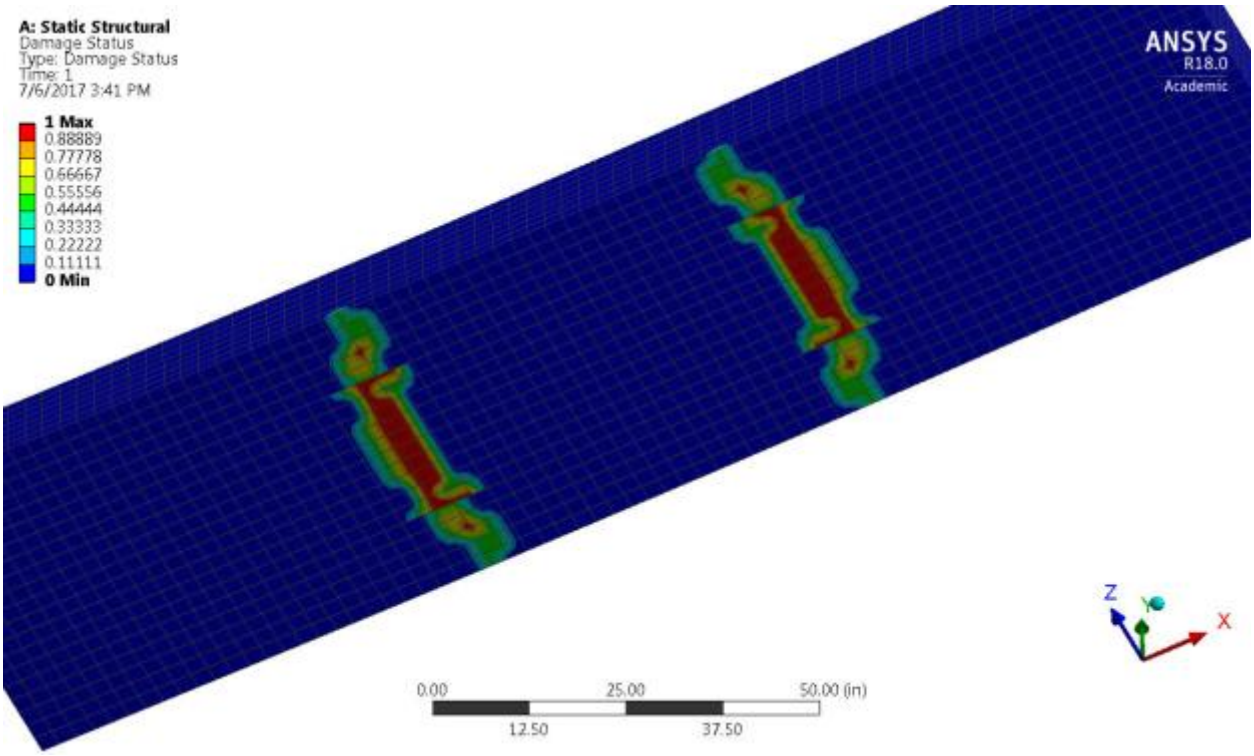

Figure 27: Damage Status

Under the given loading (45,000lbs), the maximum deformation recorded is 1.5 inches (Figure 24), the maximum bending stresses about the x-axis are 3109.6 psi in tension (bottom layer) and -4866.6 psi in compression (top layer) (Figure 25). The highest shear stresses the mat experiences about the XY plane are 125.2 psi and -102.6 psi (Figure 26). Due to pure bending, there is no shear stresses in the middle third of the span. Due to the stress limits being exceeded in bending (3109.6 psi > 2789 psi and 4866.6 psi >3940 psi), damage occurs around the location of the applied line pressures at the bottom layer which is in tension (Figure 27).

A smaller load of 30, 000 lbs. was applied to the same mat in order to perform a comparison with the previous 5-ply CLT model. Under this total pressure, the maximum deformation recorded is 0.998 inches, the maximum bending stresses about the z-axis are 2203.1 psi in tension and -3139.7 psi in compression. The highest shear stresses the mat experiences about the YZ plane are

118.5 psi and -90 psi. In this case, no damage occurs in the mat since neither the bending or shear stresses were exceeded (2203.1psi < 2789 psi and 3139.7 psi < 3940 psi for bending and 118.5 psi <1300 psi). The analysis results of the 7-ply CLT mat are summarized in Table 7.

Table 7: 7-layer CLT mat analysis results

Total Load Applied		Results
30 000 lbs	Deformation (in)	0.99847
	Damage	No
	Normal Stresses (psi)	2203.1
		-3139.7
	Shear Stresses (psi)	118.5
		-90
45 000 lbs	Deformation (in)	1.5
	Damage	Yes
	Normal Stresses (psi)	3109.6
		-4866.6
	Shear Stresses (psi)	125.2
		-102.6

4.3. Traditional wood mat with steel rods

Southern Yellow Pine No.2 wood member with the following parameters and conditions was built and analyzed.

-Total span of 185 in. (Figure 28)

-Total thickness of 12 in. (Figure 28)

-Assembly of 4 pieces of wood 11.1875 in. x 12 in. with 4 1-in. diameter A36 steel rods placed along the length of wood

-Simply supported at the bottom far ends of the member (Figure 28)

-Friction contact applied to the surfaces of wood (friction coefficient =0.2)

-Pressure applied as two equal line pressures at each third of its span (Figure 30)

A total pressure of 75,000 lbs. was applied and the analysis results were recorded and analyzed (Figure 31-37). Figure 28 shows the geometry of the traditional wood mat. Figure 29 and Figure 30 show the meshed model and the loading pattern respectively

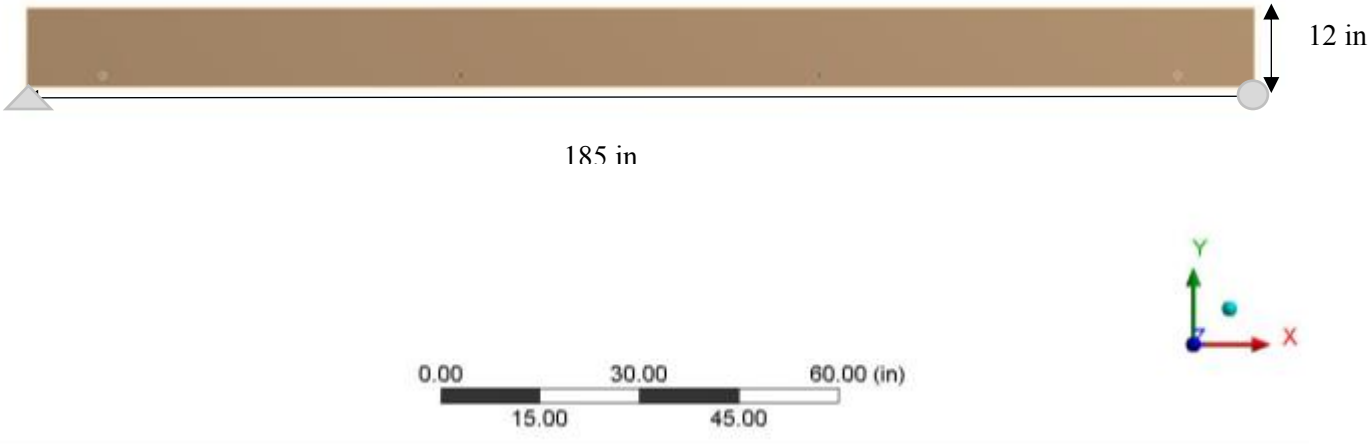

Figure 28: Geometry of wood mat

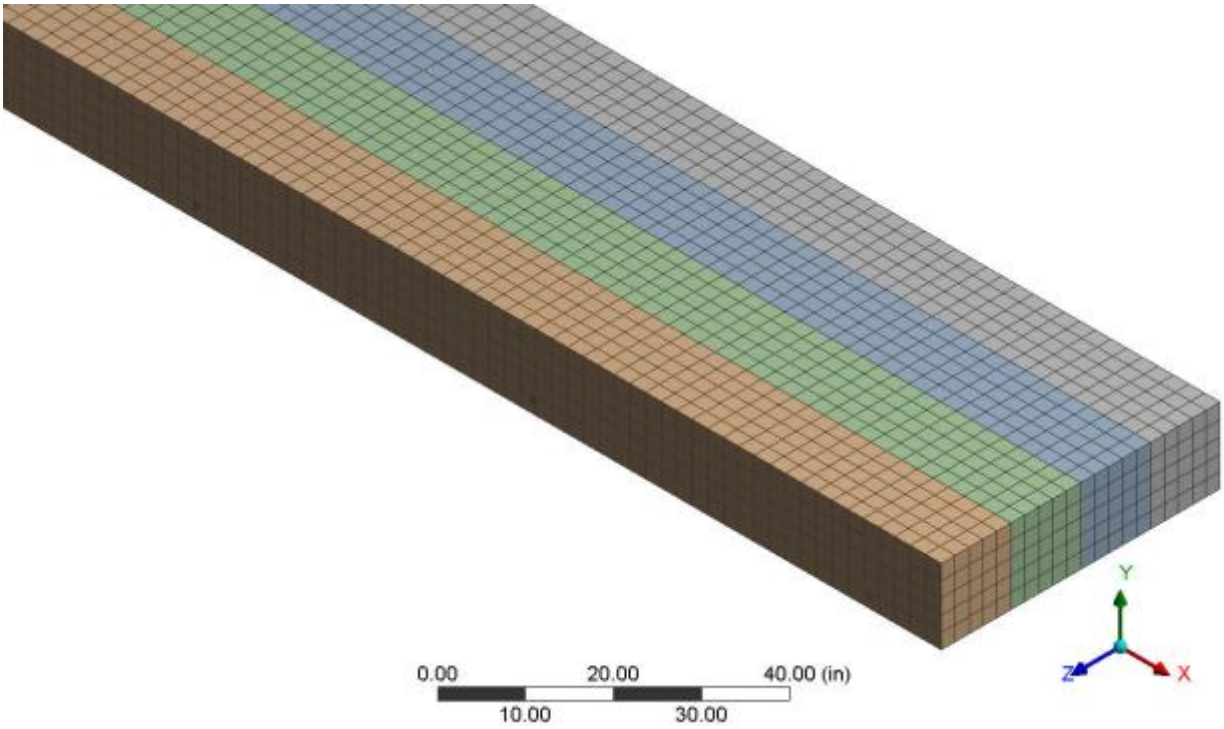

Figure 29: Meshed Model

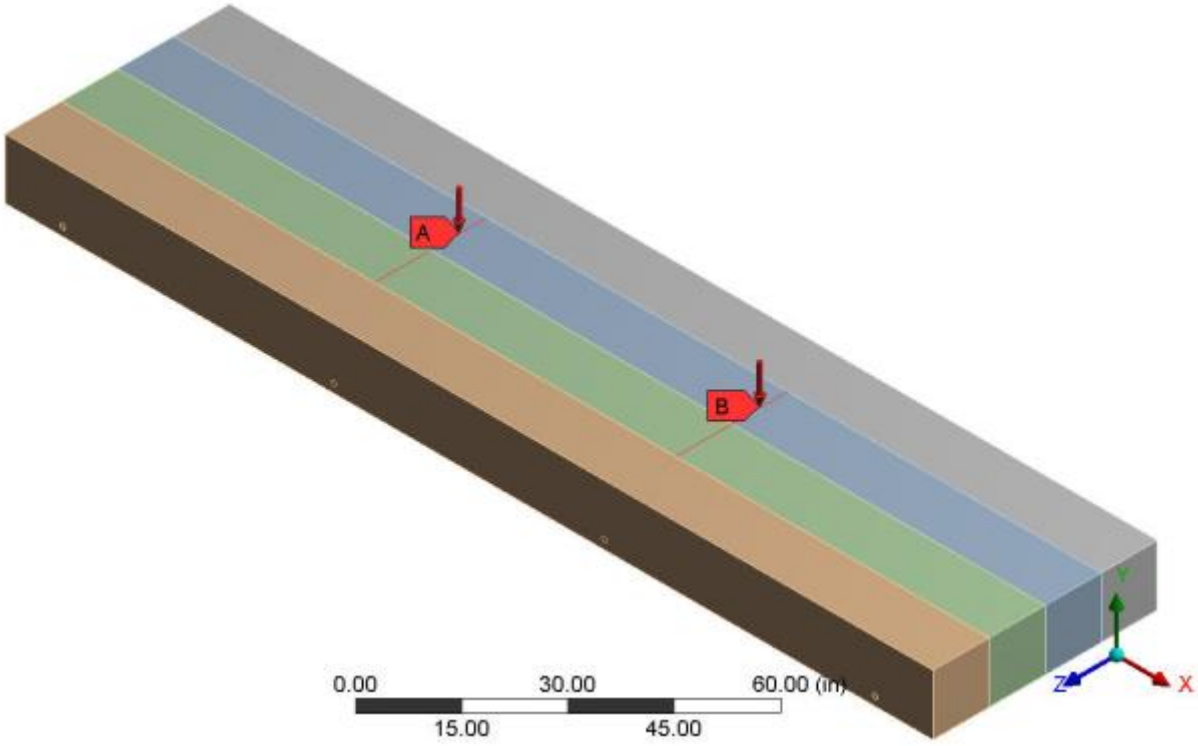

Figure 30: Loading

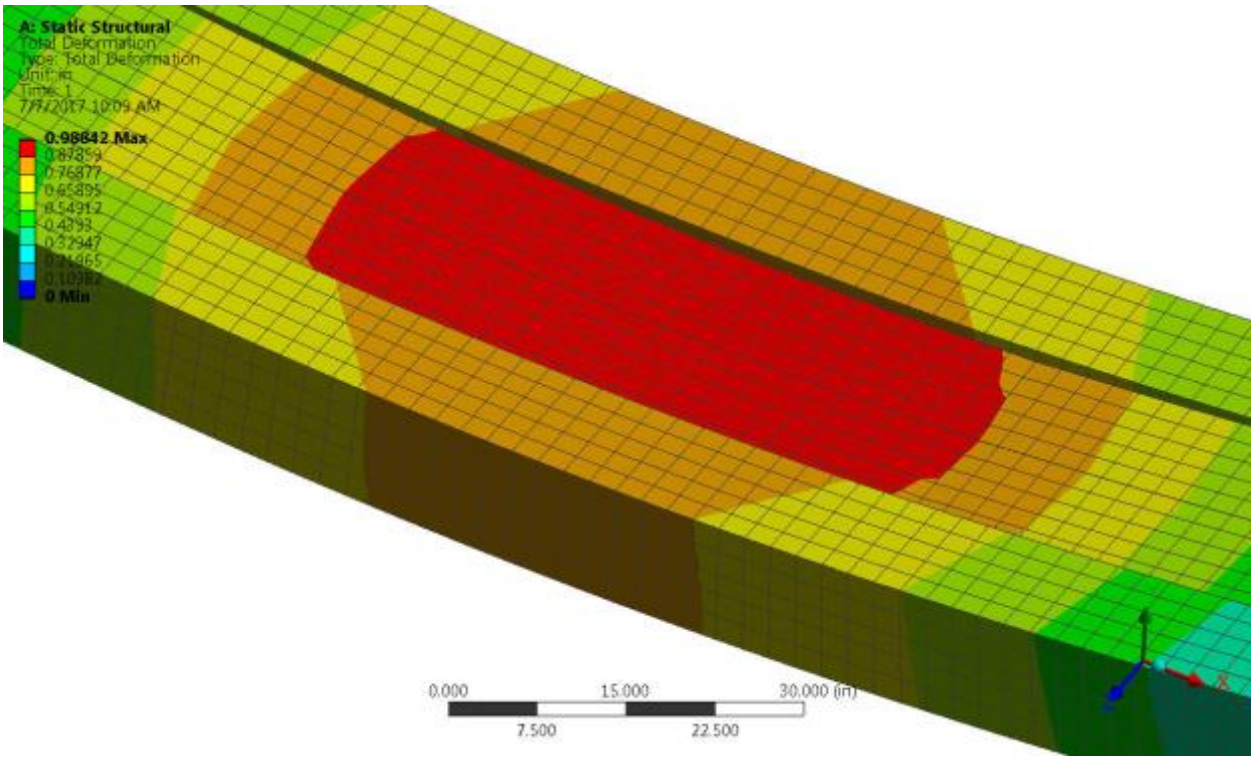

Figure 31: Deflection results of wood

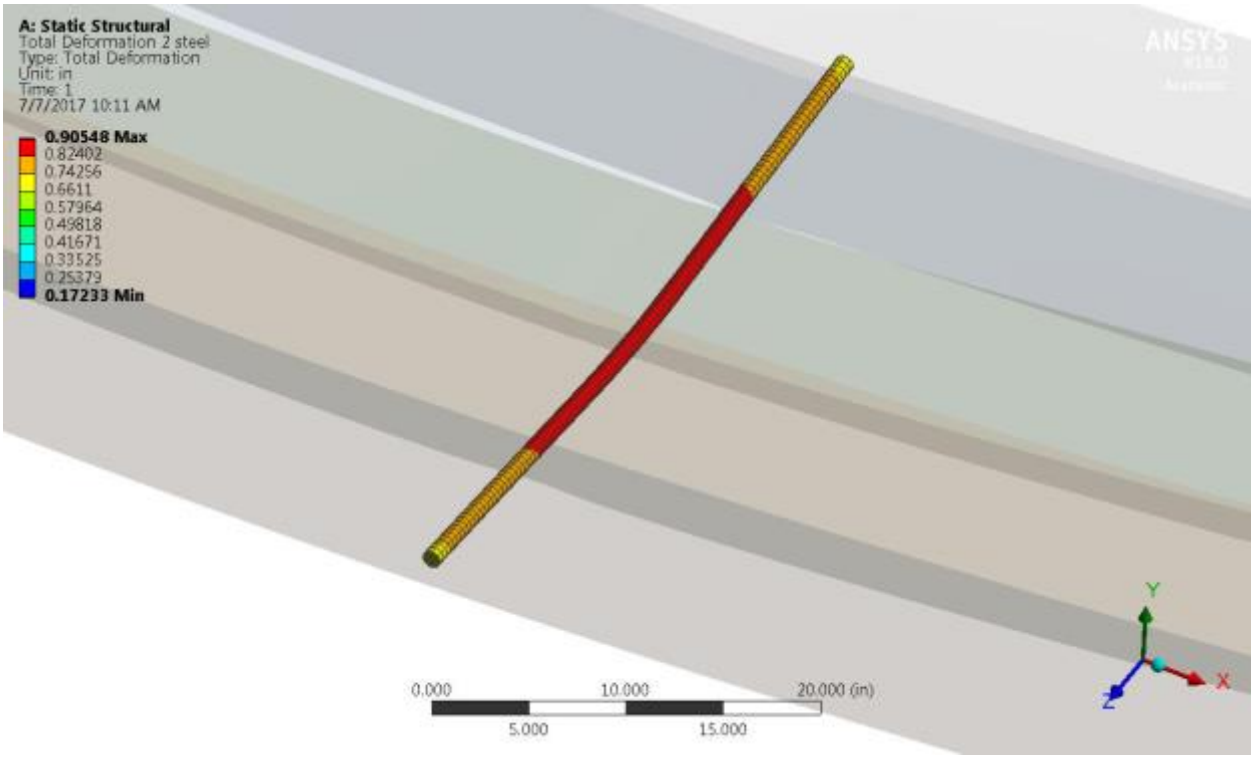

Figure 32: Deflection results of steel

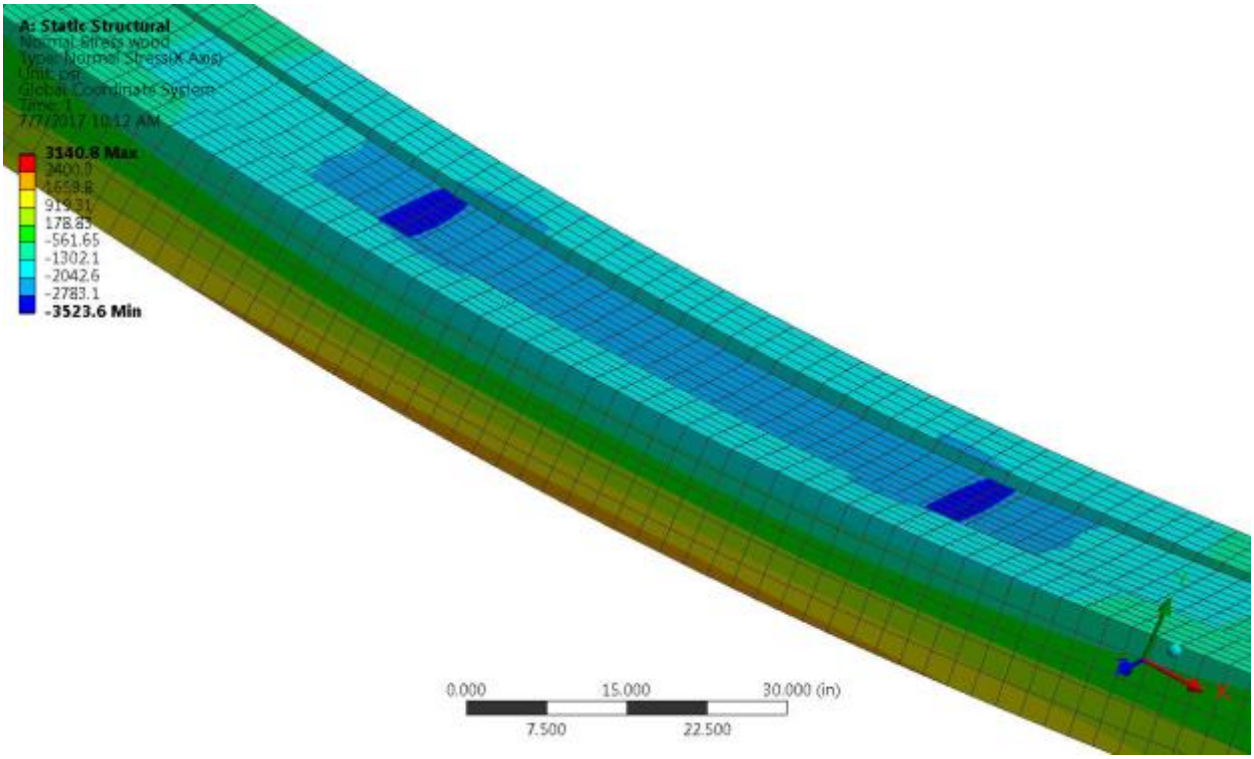

Figure 33: Normal Stresses of wood (x-axis)

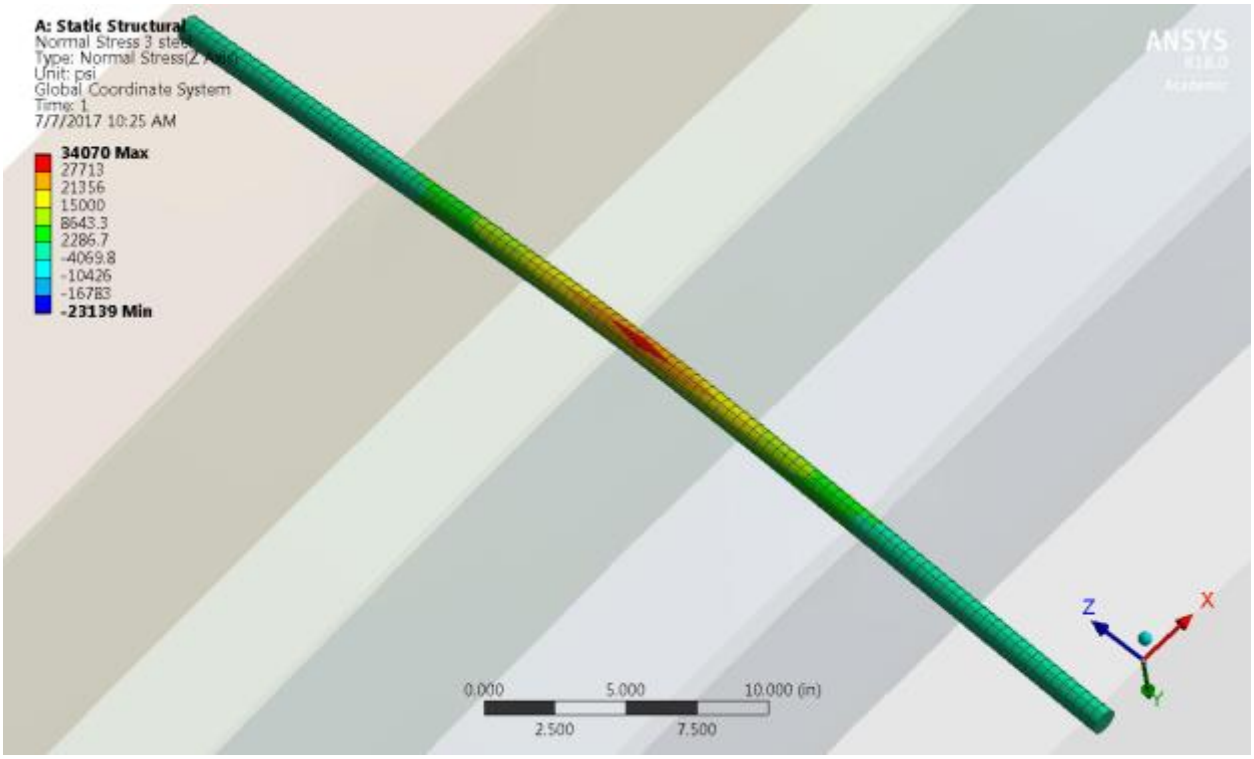

Figure 34: Normal Stresses of steel (z-axis)

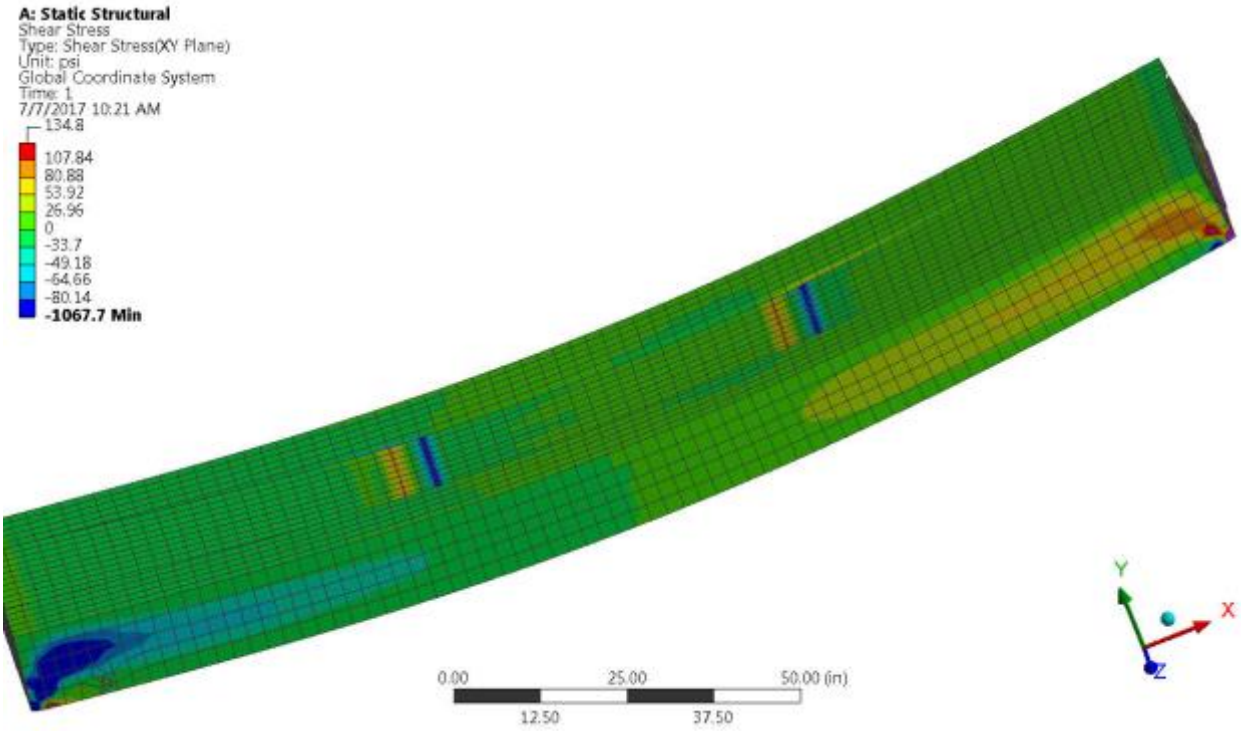

Figure 35: Shear Stresses of wood (XY plane)

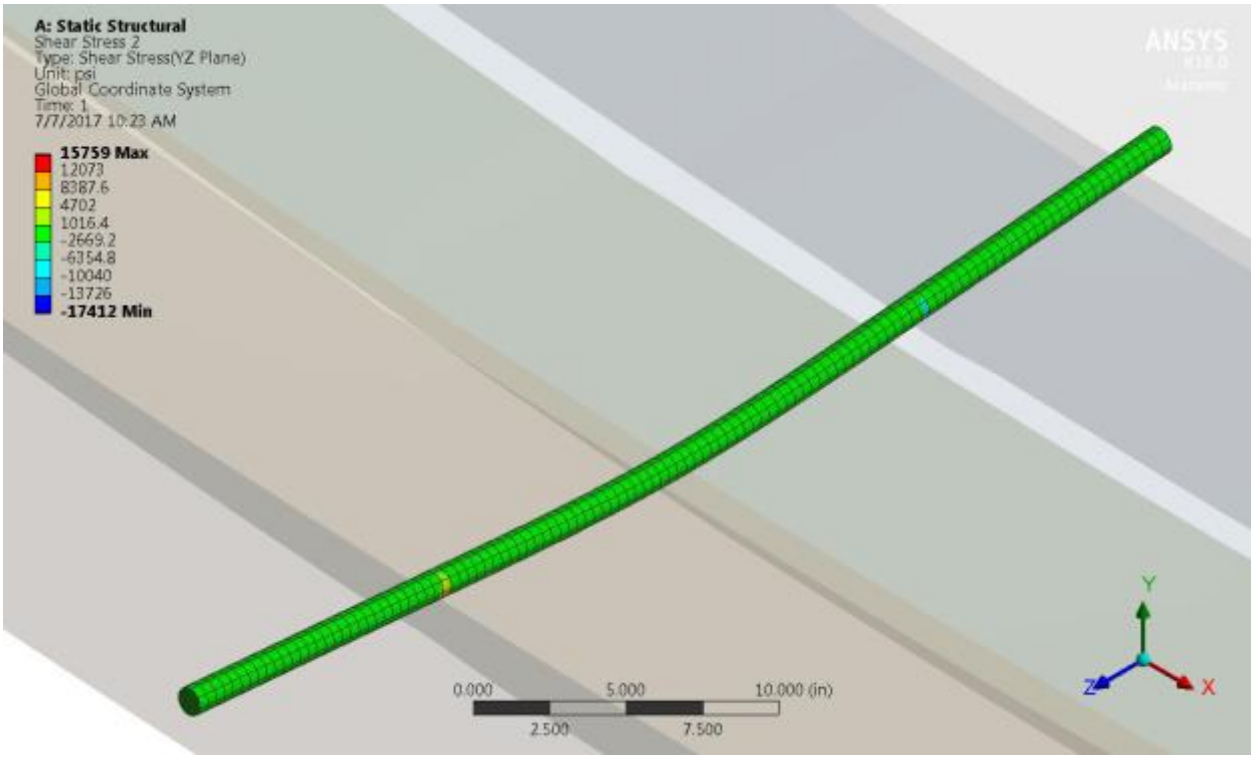

Figure 36: Shear Stresses of steel (YZ plane)

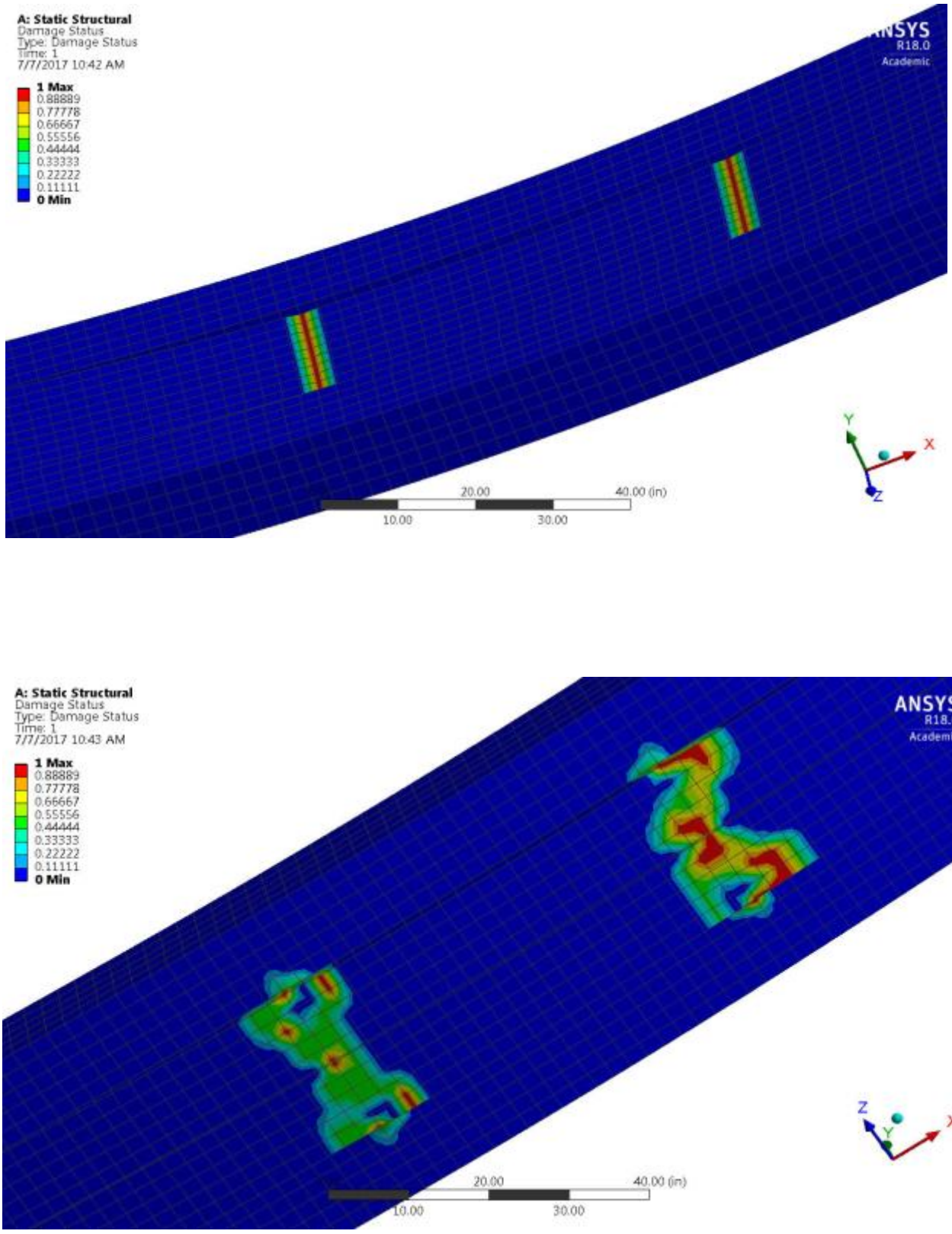

Figure 37: Damage Status of wood (Top and Bottom)

Due to friction contacts applied vertically between pieces of wood, the middle two layers of where the pressure was applied, experience more deformation and higher stresses. They appear to split apart from the other two layers (Figure 31). The maximum normal stresses occurring in wood are 3140.7 psi in tension and -3523.5 psi in compression (Figure 33) and 34069 psi and -23139 psi in steel (Figure 34). The wood deflects more than the steel rods: 0.988 in. (Figure 31) compared to 0.905 in. in steel (Figure 32). The maximum shear stresses that wood experiences are 134 psi and -80.14 psi (Figure 35), whereas the maximum shear stresses in steel are much higher than in the wood, 15,759 psi and -17,411 psi (Figure 36). From NDS Supplement 2012 Table 4B [6], allowable reference design values for bending and shear of Southern Pine No. 2 are F_b=1100 psi and F_v=175 psi respectively. The damage in the wood occurs due to the bending stresses exceeding allowable values (3140.7 psi> 1100 psi) (Figure 37). Stresses in steel do not exceed the ultimate stress values which is 66717 psi for A36 steel (34069 psi <F_u=66717 psi). From this analysis, it can be concluded that wood fails prior to the steel rods. These results are summarized in Table 8. In order to perform a comparison between different members a total load of 30,000 lbs. was applied to the traditional wood model and the analysis results in wood were recorded (Table 8). Damage occurs in wood under applied load of 30,000 lbs. due to wood failing in bending. (1570.2 psi > Fb= 1100 psi)

Table 8: Analysis results of wood and steel in a traditional wood model

Total Load Applied	Results	Wood	Steel
30,000 lbs	Deformation (in)	0.389	0.322
	Normal Stresses (psi)	1570.2	13162
		-1897.7	-9375.5
	Shear Stresses (psi)	76.3	1677.2
		-60	-1532.1
	Damage	Yes	N/A
75,000 lbs	Deformation (in)	0.988	0.905
	Normal Stresses (psi)	3140.7	34069
		-3523.5	-23139
	Shear Stresses (psi)	134	15759
		-80.14	-17411
	Damage	Yes	N/A

4.4. Comparison of Traditional model of wood and CLT

A comparison between 5-ply, 7-ply and traditional wood model was carried out. All models consist of Southern Yellow Pine (SYP) No.2 Material and were analyzed under same load case; two line pressures at each third of the span. The models were treated up to failure while gradually increasing the total load applied until damage is observed in the models. The first failure load was identified and recorded. Table 9 summarized all the dimensions for each model as well as the first damage load.

Table 9: Comparison between 5-ply, 7-ply CLT and traditional wood mat

	CLT 5-ply	CLT 7-ply	Traditional Wood Model with steel rods
Span (in)	185	185	185
Thickness (in)	6.875	9.625	12
Width (in)	44.75	44.75	44.75
First damage load (lbs)	25,000	43,000	23,500

First, the models are considered under the same loading to compare their maximum deformations and stresses reached. Under the total load of 30,000 lbs, the deformations reached in the 5- layer CLT, 7-layer CLT and traditional wood model are 2.97in, 0.99 in and 0.389 in respectively. Under this load the 5-layer CLT and traditional model fail, whereas the 7-layer CLT deforms without experiencing any damage at the same load. The maximum bending stresses are 3153.7 psi in the 5 layer CLT, 2203.1 psi in the 7-layer CLT and 1570.2 in the traditional wood model, whereas the maximum shear stresses reach 79.8 psi, 118.5 psi and 56.3psi in each model respectively. These stresses exceed the allowable stress limits in bending in the 5 layer CLT (3153.74 psi > 2789 psi), and the traditional wood model (1570.2psi > Fb=1100 psi from NDS) but not in the 7 layer CLT Model (2203.1psi < 2789psi). The models which experience damage fail in bending, not in shear. The shear stresses are still within allowable values under considered loading for all three models.

Next, the first failure load was recorded for each mat. Comparing the three models, it can be concluded that the traditional wood mat with rods, fails under a lower load (23,500 lbs) than the CLT models (25,000 and 43,000 lbs). Regardless of the different thicknesses of the models, (traditional model thicker than the CLT models) it is obvious that the CLT models (both 5 and 7 layers) can sustain more load without experiencing damage. This is a benefit of using CLT over the traditional wood mats with steel rods due to its higher strength. Another aspect to take into consideration in the comparison of two models is the weight and sustainability of the structures. CLT is much lighter weight than the traditional wood mats with steel rods which makes it more sustainable, cost effective and more applicable than the traditional rodded mats.

CHAPTER 5: CLT DESIGN PROCEDURE

5.1. Crane Mats Model Verification

The main objective of this study is to develop a design procedure for CLT mats. David Duerr published a design guide on his book "Mobile Crane Support Handbook" [7]. Chapter 4 of this study focuses on the crane mat behavior placed on soil and the interaction between soil and the mat. At certain loads, this system can be approached as "a beam on an elastic foundation" problem, yet this does not represent a realistic solution considering the non-linearity and mechanical properties of soil such as ultimate bearing pressure. Design methods were developed to predict the behavior of crane mats based on the effective bearing length of the crane mat and the balanced mat analysis method [7]. Two approaches were used to calculate the effective bearing length of the mat: based on the ground bearing capacity and based on the mat strength where the effective length is assumed initially and then adjusted based on allowable stresses. The balanced mat analysis method utilizes both the mat strength and the ground bearing capacity and balances them. The performance of the balanced mat analysis method can be assessed by performing a failure analysis of a crane mat to determine the actual capacity. A crane load vs mat bending stress curve was developed under given loads. The same analysis was performed using nonlinear finite element analysis to compare results and validate the FE model.

A standard 12 in. x 4 ft. x 20 ft. hardwood (Douglas Fir-Larch) timber crane mat centrally loaded by a 24" wide outrigger float was placed on soil whose ultimate bearing capacity is 10,000 psf with a factor of safety of 2.0 that leads to an allowable soil pressure of 5,000 psf (Figure 38). In the simple crane arrangement shown in Figure 38, L_c is the cantilevered length of the mat, L_{eff}

or L_{reqd} is the effective bearing length of the mat and P is the applied load on the crane mat through the outrigger float.

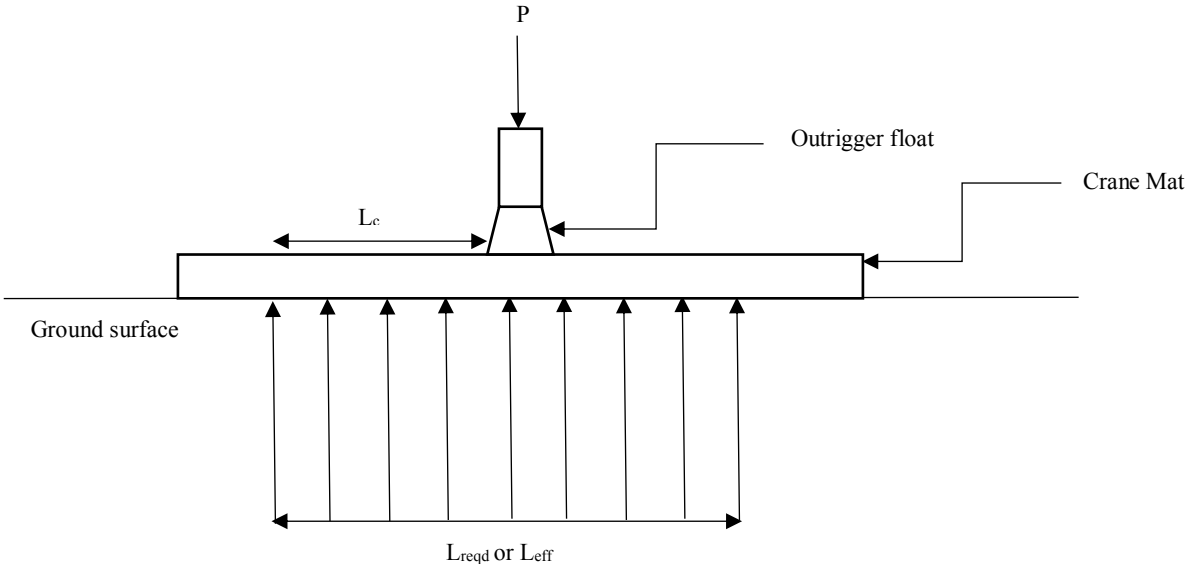

Figure 38: Simple crane mat arrangement

To develop a 3D finite element model, the material properties of Douglas Fir-Larch were determined first from NDS Supplement 2012 (National Design Specification) [6] and Wood Handbook [3]. From NDS Supplement 2012 Table 4A [6], modulus of elasticity (E_{major}) was obtained for Douglas Fir Larch No.2 wood species (E=1,600,000 psi). Taking into account, the relationships of the elastic material properties of Douglas Fir-Larch documented in the Wood Handbook (Table 5.1) [3], the rest of the elastic material properties (moduli of elasticity, E and shear moduli, G) were obtained as shown in Equations 8-12.

These material properties were derived under the assumption that the major strength axis of the grains is x-axis, so E_x=1,600,000 psi. The radial direction of grains is the y-axis and the minor strength axis is the z-axis.

$\frac{E_z}{E_x} = 0.05$ (8) E_z = 1,600,000 * 0.05=80,000 psi

$\frac{E_y}{E_z} = 0.068$ (9): E_y = 1,600,000 * 0.068 = 108,800 psi

$\frac{G_{xy}}{E_x} = 0.064$ (10): G_{xy} = 1,600,000 * 0.064 = 102,400 psi

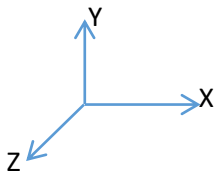

$\frac{G_{xz}}{E_x} = 0.078$ (11): G_{xz} = 1,600,000 * 0.078 = 124,800 psi

$\frac{G_{xz}}{E_x} = 0.007$ (12): G_{xz} = 1,600,000 * 0.007= 11,200 psi

The Poisson's Ratios (v) of Douglas-fir for all directions was obtained from Table 5.2 of the Wood Handbook (Table 10). The non-linear material properties of wood (maximum stress limits) were obtained from Table 5.3b of the Wood Handbook [3]. All material properties used to model Douglas-fir are summarized in Table 10.

Table 10: Linear and nonlinear material properties of Douglas Fir-Larch wood

Orthotropic Elasticity	Value	Unit
Young Modulus X direction	1,600,000	psi
Young Modulus Y direction	108,800	psi
Young Modulus Z direction	80,000	psi
Poisson Ratio XY	0.292	
Poisson Ratio YZ	0.39	
Poisson Ratio XZ	0.449	
Shear Modulus XY	102,400	psi
Shear Modulus YZ	11,200	psi
Shear Modulus XZ	124,800	psi
Orthotropic Stress Limits	Value	Unit
Tensile X direction	7,500	psi
Tensile Y direction	300	psi
Tensile Z direction	300	psi
Compression X direction	-3,610	psi
Compression Y direction	-460	psi
Compression Z direction	-460	psi
Shear XY/YZ/XZ	920	psi

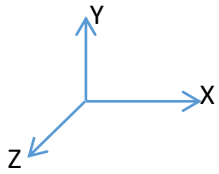

5.2. Finite Element Model and Analysis Results

The FEA model was built based on the Duerr's model description for comparison. The dimensions of wood are 12 in. x 4 ft. x 20 ft. placed in soil. Soft clay soil (Table 4) was used to support the wood mat. Symmetric boundary conditions were applied to the soil to reduce the extent of the computational model to a symmetric subsection of the overall soil system. The top nodes of the wood were restrained in order to reduce the maximum displacements in the y-direction. The two

nodes at the left end of the wood were restrained in the x-, y- and z- direction, whereas the other two nodes at the right end of the wood are restrained only in the x- and y- direction and were allowed to freely move in z-direction. Friction contacts were used between wood and soil with a friction coefficient of 0.2. The geometry and meshed model are shown in Figure 39 and Figure 40 respectively.

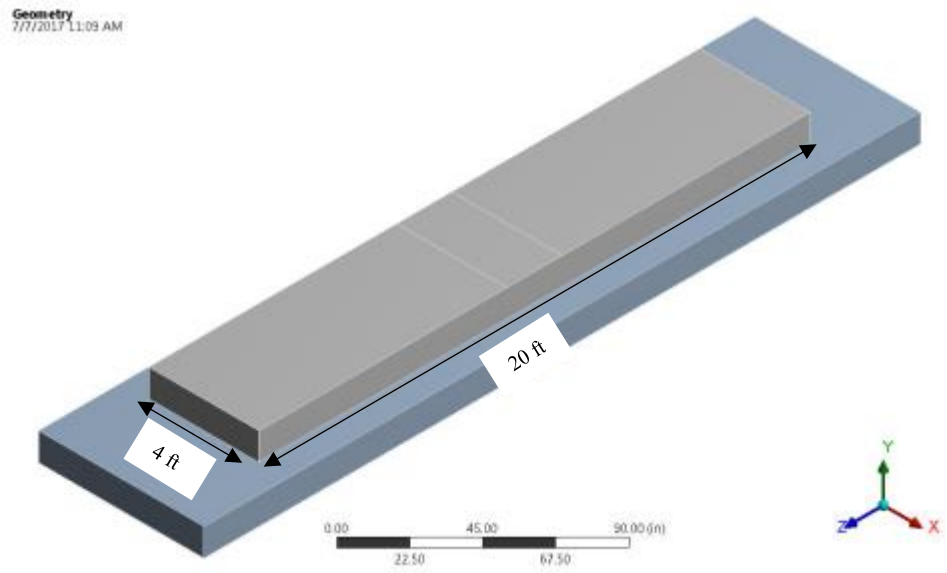

Figure 39: Geometry of wood supported by soil

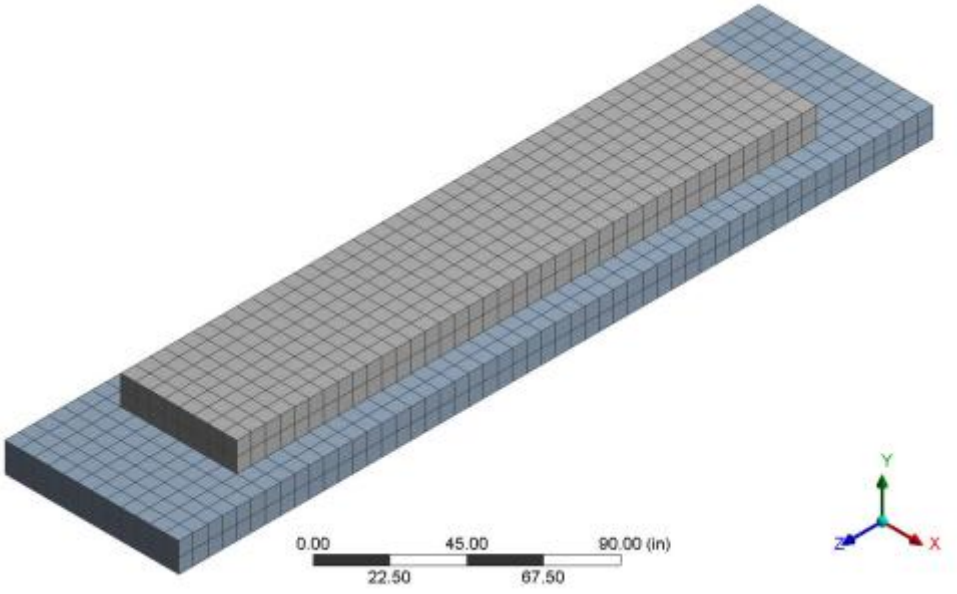

Figure 40: Meshed model

A total ultimate load of 372,000 lbs was initially applied and distributed as shown in Figure and various other loads were applied to compare results in the load-bending stresses curve between Duerr's Model and FEA. Figure 41 shows the boundary conditions on the wood and soil as well as the applied load.

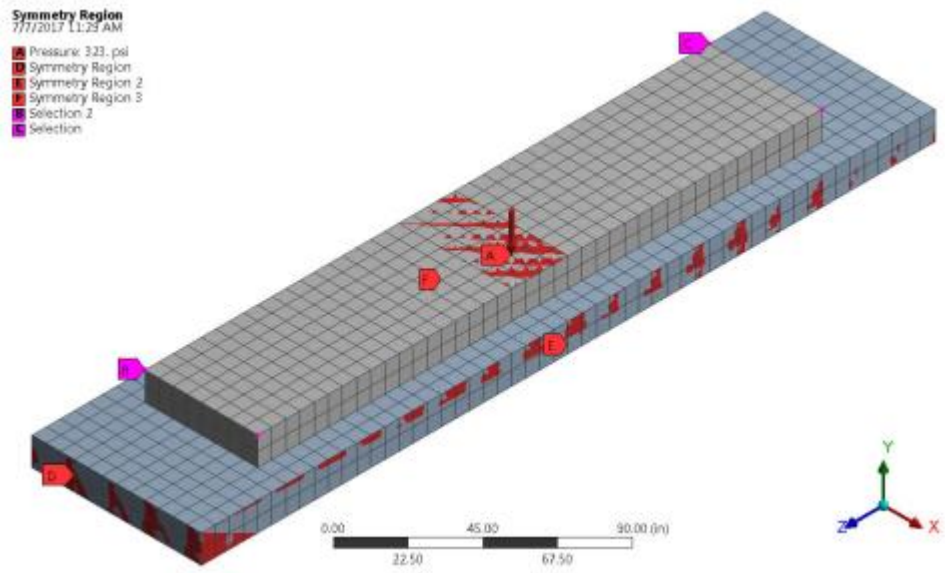

Figure 41: Boundary conditions and Loading in the combined model

Based on the geometry and loading, the following results were obtained (Figure 42-47):

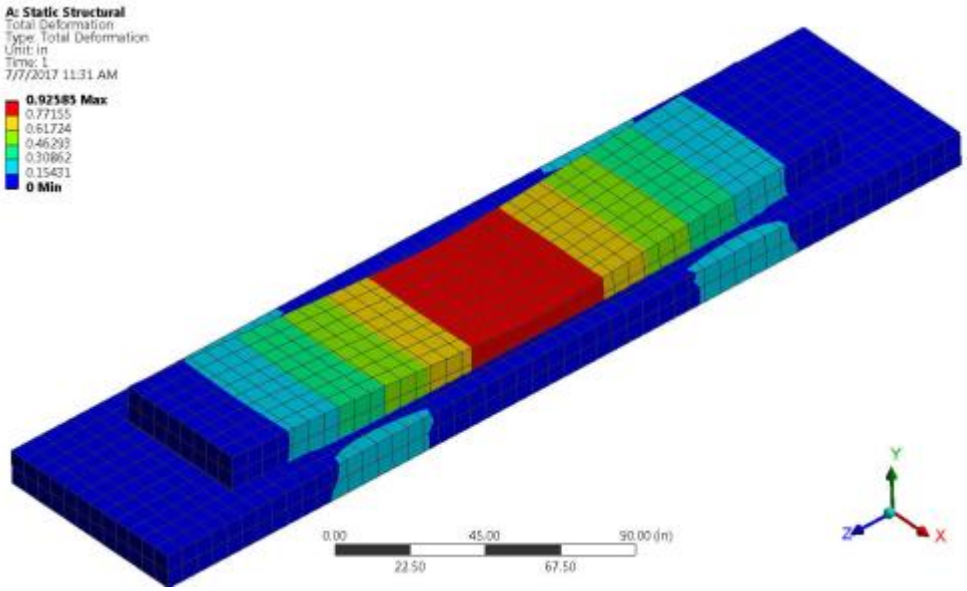

Figure 42: Deflection Results in wood and soil

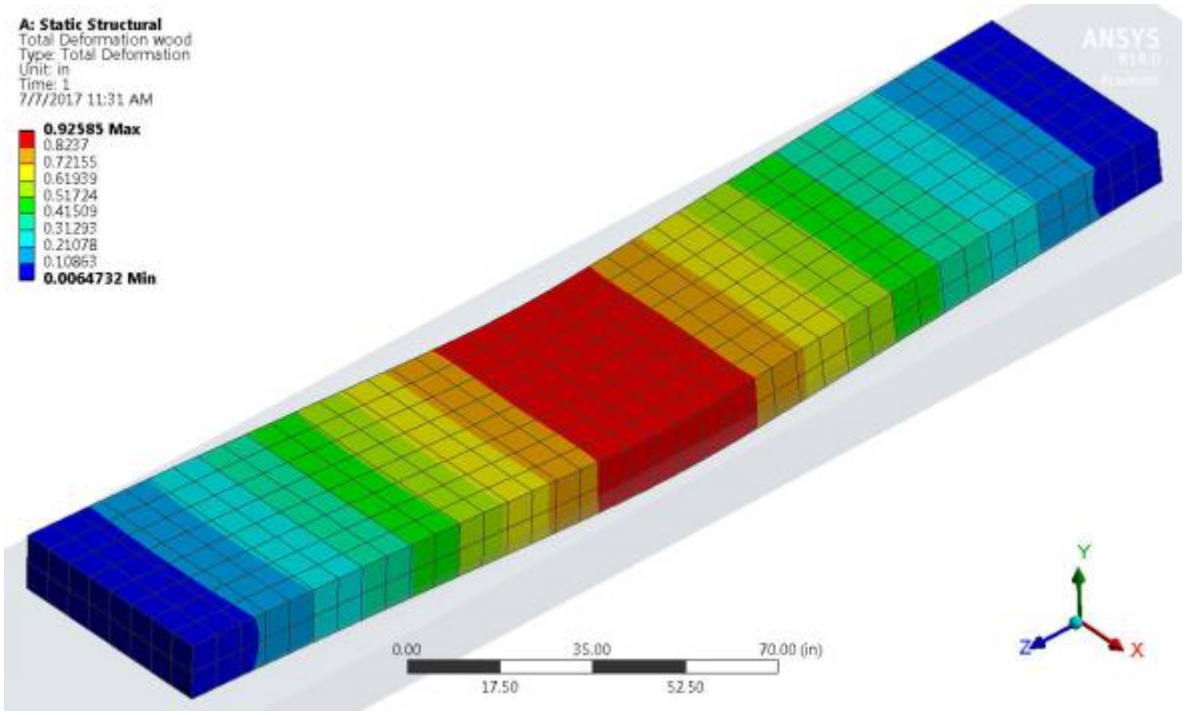

Figure 43: Deflection results in wood

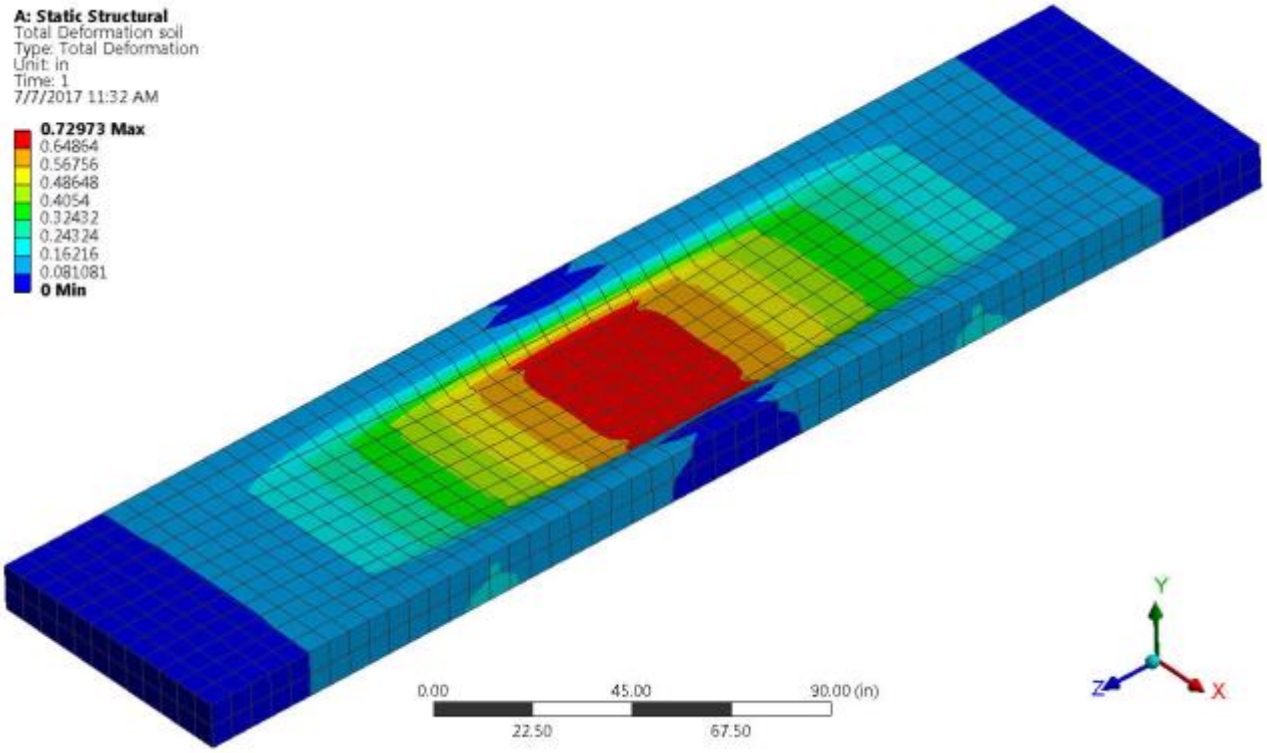

Figure 44: Deflection results in soil

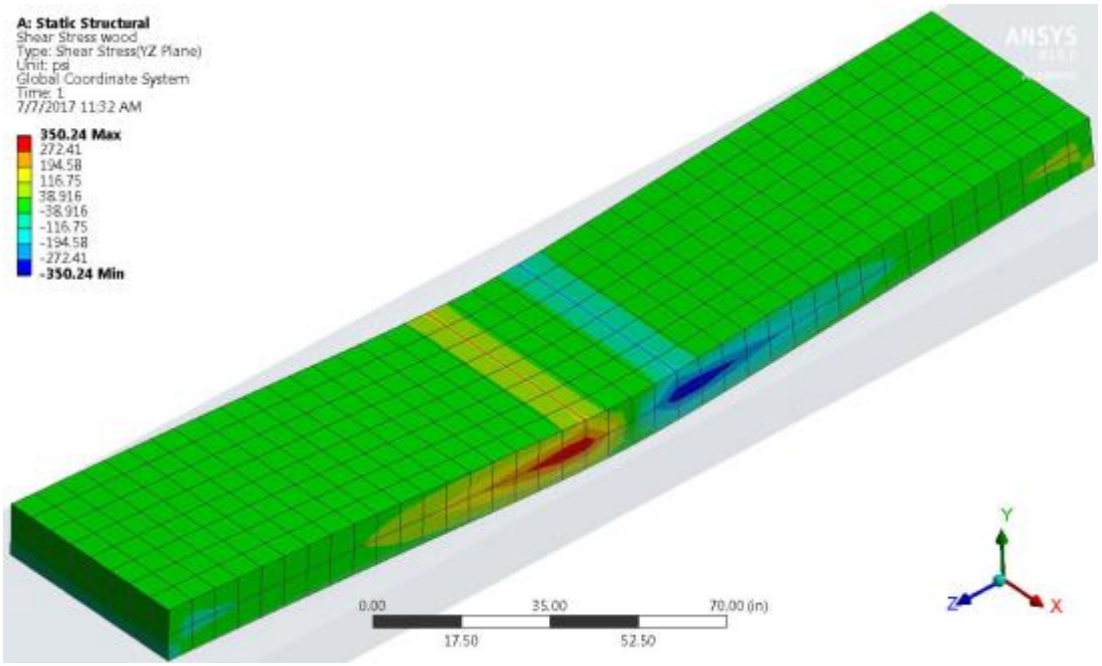

Figure 45: Shear stresses in wood (YZ plane)

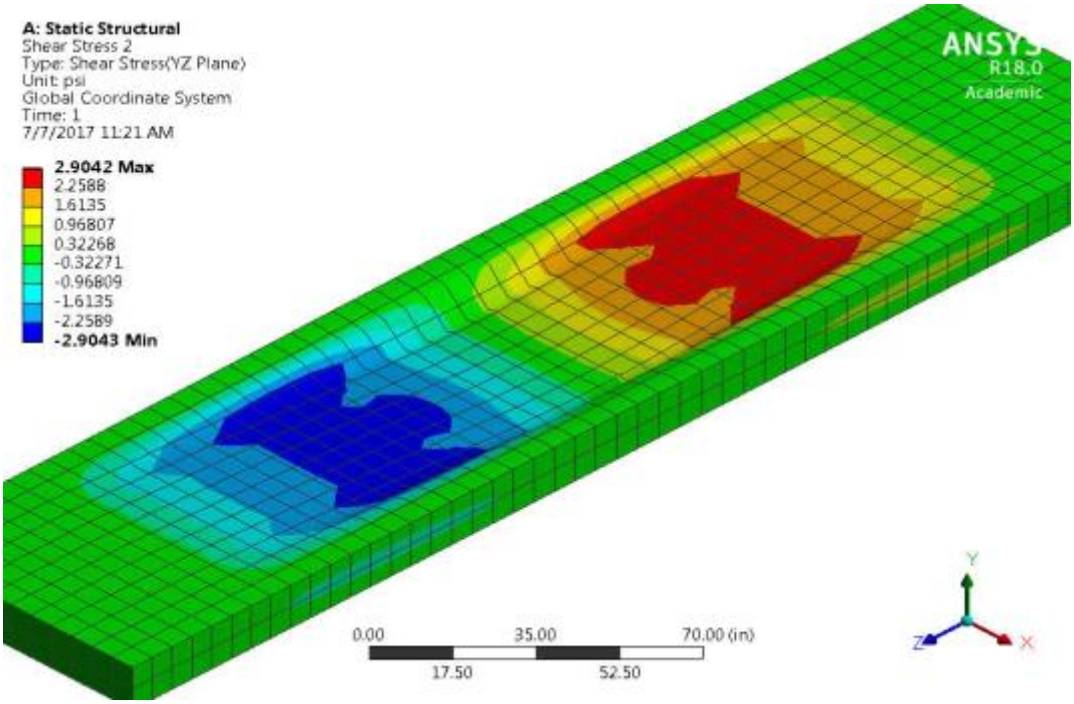

Figure 46: Shear stresses in soil (YZ plane)

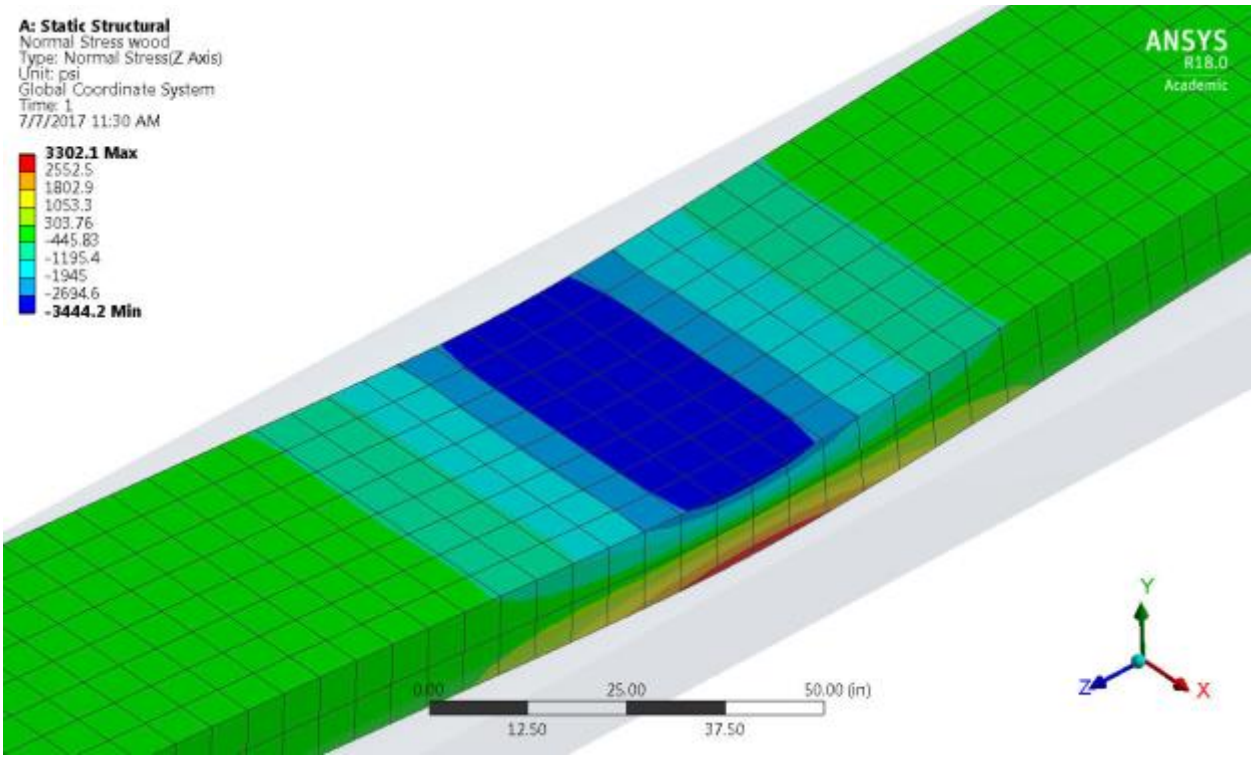

Figure 47: Normal stresses in wood (z-axis)

The maximum deflections wood and soil experience are 0.92 in. and 0.72 in. respectively (Figure 43 and Figure 44). The shear stresses are higher in the wood than the soil (Figure 45, 46) and there are no shear stresses recorded in the middle, due to the combined model being in pure bending. The normal stresses in wood are found to be 3302.1 psi and -3444.2 psi in tension and compression (Figure 7). The top surface of the wood is in compression and the bottom surface is in tension.

Additional loads were applied to the combined model and the bending stresses were recorded and plotted for each applied load. The load-bending stress curve obtained from FEA was compared to Duerr's procedure results (Figure 48) [7].

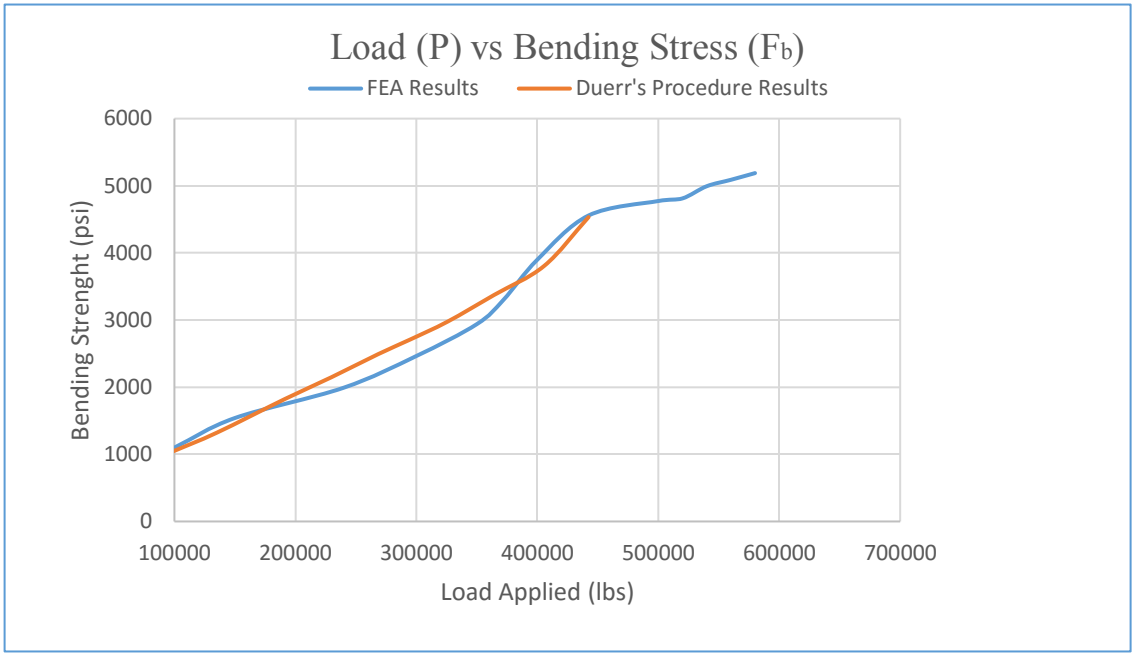

Figure 48: Load vs Bending Stresses Curves (Handbook vs FEA Results)

As shown in Figure 48, the finite element results were verified by comparing them with Duerr's Handbook load-bending stresses curve [7] for the same configuration obtained from FEM. As can be observed from the curves, there is a very good agreement between the FEA and Handbook's data. The FEA results present a reliable model and compares well with the Duerr's results. According to Duerr's elastic analysis of this mat (Fig 4.6, pg 103), the ultimate bending stresses reached at a 372,000 lbs. are 3380 psi [7], whereas from the FEA analysis, the bending stresses experienced are 3302.1 psi. That presents a 2.3% error which can be caused due to material properties, boundary conditions, mesh size or a combination of them. Up to this load, no damage in wood and no failure in soil has been observed in the FEA model, which compares well to the elastic analysis of Duerr's approach. The load was increased to further investigate the behavior of wood. Wood experiences damage at loads higher than 450,000 lbs. The non-linear behavior of wood is presented in the curve by including analysis results for loads higher than 372,000 lbs. (Figure 48) .

5.3. Development of a CLT Design Procedure

5.3.1. Shear Analogy Method

Based on the verification in the previous section, the crane mat design methods can be modified to develop a CLT design procedure. The main differences in the design methods are related to the effective section properties of CLT compared to traditional wood as well as the allowable stress limits for bending (F_b) and shear (F_v). The Shear Analogy Method of the CLT Handbook [1], [26] and ANSI/APA PRG 320-2012 standard [5] were used to develop a general CLT procedure based on the Crane Mat Design Guidelines. The Shear Analogy Method is by far the most precise design method to identify the effective section properties of different configurations of CLT [1]. This method considers different moduli of elasticity and shear moduli of single layers of CLT and takes into consideration shear deformations. This approach gives the cross-section the sum of the inherent flexural and shear stiffness. The CLT members are characterized by effective bending stiffness (EI_{eff}) and effective shear stiffness (GA_{eff}). Two main parameters that need to be calculated are the effective section modulus (S_{eff}) for flexure and $(Ib/Q)_{eff}$ for shear. These parameters can be calculated based on Equations 13 and 14 [1].

$$S_{eff} = \frac{2EI_{eff}}{E_i h} \qquad (13)$$

where EI_{eff} =Effective bending stiffness

E_i=Modulus of Elasticity of outermost layer

h= Entire thickness of panel

$$(Ib/Q)_{eff} = \frac{EI_{eff}}{\sum_{i=1}^{n/2} E_i h_i z_i} \qquad (14)$$

where EI_{eff} =Effective bending stiffness

E_i=Modulus of Elasticity of individual layer

h_i= Thickness of an individual layer, except the middle layer, which is half its thickness

z_i=Distance from the centroid of the layer to the neutral axis, except for the middle layer, where it is to the centroid of the top half of that layer (Equation 16)

For the calculation of z_i , the distance from the centroid of the each layer to the top fiber of the section needs to be recorded (Y_i).

$$Z = \frac{\sum_{i=1}^{n}(E_i A_i)*Y_i}{\sum_{i=1}^{n}(E_i A_i)} \quad (15)$$

$$z_i = Z - Y_i \quad (16)$$

The effective bending stiffness can be calculated based on Equation 17 :

$$EI_{eff} = \sum_{i=1}^{n} E_i \, b_i \, \frac{h_i^3}{12} + \sum_{i=1}^{n} E_i A_i z_i^2 \quad (17)$$

where E_i=Modulus of Elasticity of individual layer (for layers oriented in the minor strength axis, E is divided by 30 per PRG 320-2012)

h_i= Thickness of an individual layer

z_i=Distance from the centroid of the layer to the neutral axis

b_i=Width of each layer

A_i=Area of cross-section of each layer (b_i*h_i)

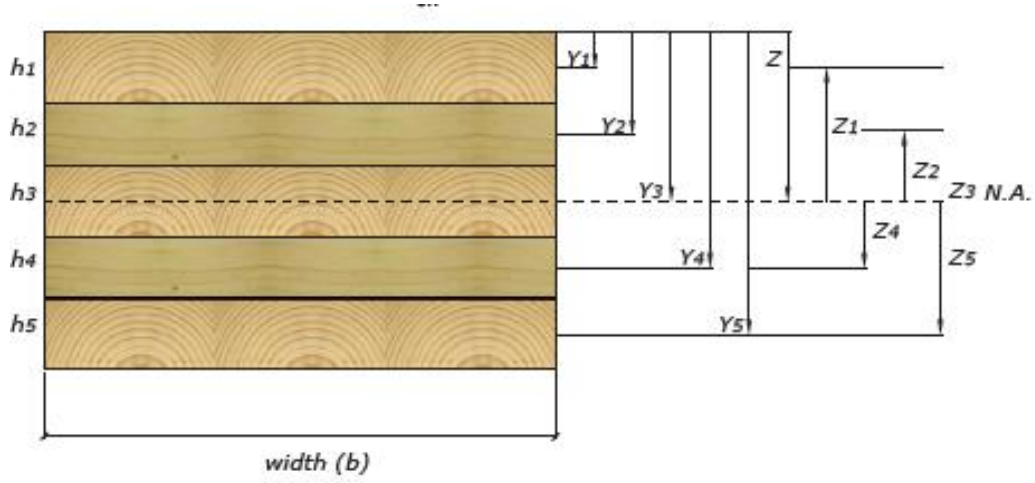

Figure 49: Effective Bending stiffness (EI_{eff}) of a 5-layer CLT

Figure 49 [26] shows the parameters needed to calculate the effective section properties of a 5-layer CLT. The thickness of an individual layer is denoted by h_i (h_1 for layer 1, h_2 for layer 2, etc.), b is the design width, and Y_i and z_i are defined in Equations 15 and 16. As an example the value for z_3 in this section is 0, since it lays on the neutral axis.

To show the steps of the CLT design procedure developed, the same crane arrangement of Figure 38 was taken into consideration and replaced by V1 Grade CLT, which is made out of No.2 Douglas fir-Larch lumber in all parallel layers and No.3 Douglas fir-Larch in all perpendicular layers (PRG 320-2012 Table A1) [3]. Three design methods of the Duerr's procedure [7] were modified for a 5-ply CLT and shown in details in the design examples below.

5.3.2. CLT Design Procedure

Three different design methods were adapted from the Crane Mat Handbook [7] to develop a CLT design procedure. The design methods used are developed by calculating the effective bearing length of the mat based on ground bearing capacity and mat strength and by using the Balanced Mat Analysis method. All parameters used in these methods are defined below:

P = crane load applied to the mat ;

W = self-weight of the mat;

q_a = allowable ground bearing pressure;

A_{reqd} = required mat bearing area;

B = mat width;

L_{reqd} / L_{eff}= required /assumed effective bearing length of the mat;

L_{total} =total length of the mat;

C = bearing width of the outrigger pad;

L_c = cantilevered length of the mat;

q = ground bearing pressure due to P;

q_t = calculated total ground bearing pressure;

M = calculated bending moment in the mat;

M_n = allowable moment in the mat;

f_b = bending stress due to M;

F_b = design bending stress modified by applicable adjustment factors per CLT handbook [1];

V = calculated shear in the mat;

V_n= allowable shear in the mat;

d = mat total depth or thickness;

f_v = shear stress due to V;

F_v= design shear stress modified by applicable adjustment factors per CLT handbook [1];

$(EI)_{eff}$ = effective bending stiffness;

$(Ib/Q)_{eff}$ = effective shear parameter;

S_{eff} = effective section modulus;

The first design method is based on the calculation of the effective bearing length of the mat based on ground bearing capacity. The required crane mat area is calculated by dividing the total applied load and the self-weight of mat by the allowable ground bearing pressure. The required effective bearing length of the mat is obtained by dividing the calculated area with the width of the mat, which is used to calculate the bending and shear stresses in the mat [7]. If the calculated stresses in the mat are equal to or less than the corresponding allowable stresses, the mat is acceptable for the applied load and ground bearing capacity. Equations 18-26 show the steps followed to apply this method.

1. Calculate mat dead weight

$$W = B * d * L_{total} * density_{timber} \quad (18)$$

2. Calculate the required effective area

$$A_{reqd} = \frac{P+W}{q_a} \quad (19)$$

3. Calculate the required effective bearing length of the mat

$$L_{reqd} = \frac{A_{reqd}}{B} \quad (20)$$

4. Calculate the cantilevered length of the mat

$$L_c = \frac{L_{reqd} - C}{2} \quad (21)$$

5. Calculate ground bearing pressure due to P

$$q = \frac{P}{L_{reqd} B} \quad (22)$$

6. Calculate bending moment in the mat

$$M = \frac{(qB)L_c^2}{2} \quad (23)$$

7. Calculate bending stress due to bending moment (M) and compare to allowable bending stress, F_b

$$f_b = \frac{M}{S_{eff}} \quad (24)$$

8. Calculate shear in the mat

$$V = (qB)(L_c - d) \quad (25)$$

9. Calculate shear stress due to calculated shear (V) and compare to allowable shear stress, F_v.

$$fv = \frac{V}{(Ib/Q)_{eff}} \leq F_v \quad (26)$$

The second design method is based on the calculation of the effective bearing length of the mat based on mat strength. This design approach is the reverse of the first method. An effective bearing length is initially assumed and then adjusted until the resulting bending stress or shear stress reaches its corresponding allowable value [7]. Based on the adjusted effective bearing length, the ground pressure is computed. If the calculated bearing pressure is equal or less than the allowable bearing pressure, the mat is acceptable. Equations 27-34 show the steps followed to apply this method.

1. Calculate mat dead weight

$$W = B * d * L_{total} * density_{timber} \quad (27)$$

2. Assume a value for L_{eff}
3. Calculate the cantilevered length of the mat

$$L_c = \frac{L_{eff} - C}{2} \quad (28)$$

4. Calculate ground bearing pressure due to P and self-weight

$$q = \frac{P+W}{L_{eff}B} \quad (29)$$

5. Calculate bending moment in the mat

$$M = \frac{(qB)L_c^2}{2} \quad (30)$$

6. Calculate bending stresses in the mat due to calculate moment (M) and compare to the allowable bending stress, F_b. Go back to step 2 and adjust Leff until bending stresses reach the allowable value, F_b.

$$f_b = \frac{M}{S_{eff}} = F_b \quad (31)$$

7. Calculate shear in the mat

$$V = (qB)(L_c - d) \quad (32)$$

8. Calculate shear stresses due to calculated shear (V) and compare to allowable shear stress, F_v

$$fv = \frac{V}{(Ib/\,Q)_{\,eff}} \leq F_v \quad (33)$$

The design is complete when the effective bearing length has been determined in such a way that either the bending stress or the shear stress reaches its allowable value.

9. Calculate the total ground bearing pressure

$$q_t = \frac{P+W}{L_{eff}B} \leq q_a \quad (34)$$

The third design method is the Balanced Mat Analysis method which is a more practical method based on the utilization of the mat strength, the ground bearing capacity and balancing of the two parameters. The effective bearing length of the mat is calculated by taking into account the bending, shear and deflection limit and the smallest value is chosen as controlling. The bending, shear and ground bearing pressure are recalculated based on the controlling effective bearing length. The recalculated values are expressed relative to the allowable values as utilization ratios. If all the ratios are less than 1, the mat is acceptable for this application [7]. Equations 35-48 show the steps followed to apply this method.

Case 1:

1. Calculate the effective bearing length as limited by maximum bending strength (M_n)

$$M_n = F_b * S_{eff} \quad (35)$$

$$(q_a B)*L_{eff}^2 + (-2q_a BC - W)*L_{eff} + (q_a BC^2 + 2CW - 8M_n) = 0 \quad (36) \text{ ->Solve for } L_{eff}$$

Case 2:

2. Calculate the effective bearing length as limited by maximum shear strength (V_n)

$$V_n = F_v * (Ib/Q)_{eff} \quad (37)$$

$$(q_a B)*L_{eff}^2 + (-2V_n - 2q_a BC - 2q_a Bd - W)*L_{eff} + (CW + 2Wd) = 0 \quad (38) \text{ ->Solve for } L_{eff}$$

Case 3:

3. From the deflection limit of a crane mat (assuming $\Delta = 0.0075\ L_c$), calculate the cantilevered length of mat and the effective bearing length

$$L_c = \sqrt[3]{\frac{0.06\ (EI)_{eff}}{0.9\ q_a B}} \quad (39)$$

$$L_{eff} = 2L_c + C \quad (40)$$

4. Choose the controlling minimum L_{eff} value

5. With the selected controlling L_{eff} value, compute ground bearing pressure

$$q = \frac{P}{L_{eff}B} \quad (41)$$

6. With the selected controlling L_{eff} value, calculate the cantilevered length of mat

$$L_c = \frac{L_{eff} - C}{2} \quad (42)$$

7. Calculate bending moment in the mat

$$M = \frac{(qB)L_c^2}{2} \quad (43)$$

8. Calculate shear in the mat

$$V = (qB)(L_c - d) \quad (44)$$

9. Calculate the total ground bearing pressure

$$q_t = \frac{P+W}{L_{eff}B} \quad (45)$$

10. Calculate the utilization ratios for each limit state (shear, bending, and ground bearing pressure) as the actual force, stress or pressure divided by the corresponding allowable value.

$$M/Mn < 1 \quad (46)$$

$$V/Vn < 1 \quad (47)$$

$$q_t/q_a < 1 \quad (48)$$

To develop the above mentioned CLT design procedure, the section properties of the mat in the methods above were replaced with the effective section properties of CLT. In equations 24, 31 and 35 the section modulus (S) was replaced by the effective sections modulus of CLT (S_{eff}) to calculate bending stresses in the mat (f_b) in Method 1 and 2 and the allowable bending moment (M_n) in method 3. In equations 26, 33 and 37, the effective parameter $(Ib/Q)_{eff}$ was used to calculate the shear stresses (f_v) in Method 1 and 2 and the allowable shear force in the mat (V_n) in Method 3. In equation 39, bending stiffness (EI) was replaced with the effective bending stiffness of CLT, $(EI)_{eff}$. All three methods along with the calculation of the effective section properties are presented below in a design example for a 5-ply CLT mat.

5.3.3. CLT Design Example

Analyze the 5-ply V1 Grade CLT arrangement shown in Figure 35 for an outrigger load of 65,000 lbs. applied to a 4 ft. width and 20 ft. span CLT mat through an outrigger float that is 24 in. wide along the length of the mat. The allowable ground bearing pressure is 3000 psf and CLT allowable stresses in bending and shear are F_b = 900 psi and F_v = 180 psi [5]. The timber density is 50 pcf.

1. Material Properties of CLT

Material properties of V1 Grade CLT obtained from PRG 320-2012 Standard [5] are presented below. PRG 320-2012 Standard assumes that G=E/16 and that for the minor strength axis. G should be divided by 10 for rolling shear [5].

E_0=1,600,000 psi (modulus of elasticity in the major strength direction)

E_0=1,400,000 psi (modulus of elasticity in the minor strength direction)

$G_o=E_o/16$=100,000 psi (shear modulus in the major strength direction)

$G_{90}=E_0/160$=8,750 psi (shear modulus in the minor strength direction)

2. Geometry and dimensions of the CLT Mat.

The geometry is shown in Figure 46 and the dimensions are as following:

b=48 in.

$h_1=h_2=h_3=h_4=h_5$=1.375 in. which leads to h_{total}=6.875 in.

3. Calculations of the effective section properties using Shear Analogy Method are performed as following:

(a) Calculation of Z Parameter

Based on Equation 15, Z parameter was calculated in Table 11.

Table 11: Calculation of Z parameter

Layer	E_iA_i, lb.	Y_i, in.	$E_iA_iY_i$, lb.in.
1	1.056E+08	0.6875	7.260E+07
2	9.240E+07	2.0625	1.906E+08
3	1.056E+08	3.4375	3.630E+08
4	9.240E+07	4.8125	4.447E+08
5	1.056E+08	6.1875	6.534E+08
Sum	5.016E+08		1.724E+09

Z= 1.702E+09 / 4.950E+08 = **3.44 in.**

(b) Calculation of Effective bending stiffness: EI_{eff}

The calculation of the effective bending stiffness was performed based on Equations 15 and 16 and shown in Table 12. For the layers oriented in the minor strength axis (layers 2 and 4), the modulus of elasticity E is divided by 30 per PRG 320-2012 to adjust for bending perpendicular to the strong axis [5].

Table 12: Calculation of effective bending stiffness

Layer	E, psi	z, in.	$Ebh^3/12$, lb.-in.^{2}	EAz^2, lb.-in.^{2}	∑, lb.-in.^{2}
1	1600000.00	2.750	1.664E+07	7.986E+08	8.1524E+08
2	46666.67	1.375	4.853E+05	5.823E+06	6.3084E+06
3	1600000.00	0.000	1.664E+07	0.000E+00	1.6638E+07
4	46666.67	-1.375	4.853E+05	5.823E+06	6.3084E+06
5	1600000.00	-2.750	1.664E+07	7.986E+08	8.1524E+08
				Total, lb.-in.^{2}	**1.660E+09**

EI_{eff} = **1.761E+09 lbs.-in.^{2}**

(c) Calculation of Effective section modulus: S_{eff}

The calculation of the effective section modulus was performed based on Equation 13.

$$S_{eff} = \frac{2*1.660E+09}{1.6E+06*6.875} = \mathbf{301.8\ in.^3}$$

(d) Calculation of $(Ib/Q)_{eff}$ Parameter

The calculation of $(Ib/Q)_{eff}$ parameter needed for shear calculations was performed based on Equation 14 and presented in Table 13.

Table 13: Calculation of $(Ib/Q)_{eff}$ parameter

Layer	E, psi	z, in	Ehz
1	1600000	2.750	6.050E+06
2	46666.67	1.375	8.823E+04
3	1600000	0.688	1.513E+06
		∑	7.651E+06

$(Ib/Q)_{eff}$ = **216.9 in.^{2}**

4. CLT Design Methods

After the calculation of the effective section properties of the CLT mat, three methods from Duerr's design procedure were modified to solve the example presented in Section 5.3.3.

(a) Method 1: Mat Length based on ground bearing capacity

Mat dead weight: W = (6.875/12) ft. * 4 ft. * 20 ft. * 50 pcf = 2291.67 lbs.

$$A_{reqd} = \frac{P+W}{q_a} = \frac{65{,}000+2291.67}{3{,}000} = 22.43 \text{ ft.}^2$$

$$L_{reqd} = \frac{A_{reqd}}{B} = \frac{22.43}{4} = 5.61 \text{ ft.}$$

$$L_c = \frac{L_{reqd}-C}{2} = \frac{5.61-24/12}{2} = 1.8 \text{ ft.}$$

$$q = \frac{P}{L_{reqd}B} = \frac{65{,}000}{5.61*4} = 2{,}898 \text{ psf}$$

$$M = \frac{(qB)L_C^2}{2} = \frac{(2898*4)1.8^2}{2} = 2{,}715{,}672 \text{ lbs.-ft} = 226{,}306 \text{ lbs.-in.}$$

$$f_b = \frac{M}{S_{eff}} = \frac{226{,}306}{301.8} = 750 \text{ psi} < F_b = 900 \text{ psi (OK)}$$

$$V = (qB)(L_c - d) = (2{,}898 *4)*(1.8\text{-}6.875/12) = 14269 \text{ lbs.}$$

$$fv = \frac{V}{(Ib/Q)_{eff}} = \frac{14{,}269}{216.9} = 66 \text{ psi} < F_v = 180 \text{ psi (OK)}$$

The calculated stresses are within allowable limits, thus the mat is acceptable for this application.

(b) Method 2: Mat Length based on mat strength

Assume L_{eff} = 6.11 ft.

W = (6.875/12) ft. * 4 ft. * 20 ft. * 50 pcf = 2291.67 lbs.

$L_c = \frac{L_{eff} - C}{2} = \frac{6.11 - 24/12}{2} = 2.06$ ft.

$q = \frac{P+W}{L_{eff}B} = \frac{65{,}000}{6.11*4} = 2{,}660$ psf

$M = \frac{(qB)L_c^2}{2} = \frac{(2{,}660*4)2.06^2}{2} = 270{,}911$ lbs.-in.

$f_b = \frac{M}{S_{eff}} = \frac{270{,}911}{301.8} = 898$ psi $\approx F_b = 900$ psi

$V = (qB)(L_c - d) = (2{,}660 * 4) * (2.06 - 6.875/12) = 15{,}823$ lbs.

$fv = \frac{V}{(Ib/Q)_{eff}} = \frac{15{,}823}{216.9} = 73$ psi $< F_v = 180$ psi (OK)

$q_t = \frac{P+W}{L_{eff}B} = \frac{65{,}000 + 2291.67}{6.11*4} = 2{,}753$ psf < 3000 psf (OK)

The assumed value of the effective bearing length of the mat is shown to produce a bending stress nearly equal to the allowable bending stress, a shear stress and a ground bearing pressure less than the allowable limits, and thus the mat is acceptable for this application.

(c) Method 3: Balanced mat analysis method

Case 1:

$M_n = F_b * S_{eff}/12 = 900 * 301.8/12 = 22{,}632.75$ lb-ft

$(q_aB)*L_{eff}^2 + (-2q_aBC-W)*L_{eff} + (q_aBC^2+2CW-8M_n) = 0$ ->Solving for L_{eff}=**5.932ft**.

Case 2:

$V_n = F_v * (Ib/Q)_{eff} = 180 * 216.9 = 39{,}042$ lbs.

$(q_aB)*L_{eff}^2 + (-2V_n-2q_aBC-2q_aBd-W)*L_{eff} + (CW+2Wd) = 0$ ->Solving for L_{eff}=9.784 ft.

Case 3:

$$L_c = \sqrt[3]{\frac{0.06\ (EI)_{eff}}{0.9\ q_aB}} = 48 \text{ in.} = 4 \text{ ft.}$$

$L_{eff} = 2L_c + C = 10$ ft.

The minimum L_{eff} value is 5.932 ft. (Case 1)

$$q = \frac{P}{L_{eff}B} = \frac{65{,}000}{5.932*4} = 2{,}740 \text{ psf}$$

$$L_c = \frac{L_{eff}-C}{2} = \frac{5.932-24/12}{2} = 1.966 \text{ ft.}$$

$$M = \frac{(qB)L_c^2}{2} = \frac{(2{,}740*4)1.966^2}{2} = 21{,}811 \text{ lbs.-ft}$$

$M/Mn = 21{,}811/22632.75 = 0.936 < 1$ (OK)

$V = (qB)(L_c - d) = (2{,}740 * 4) * (1.966 - 6.875/12) = 15{,}268$ lbs.

$V/Vn = 15{,}268/39{,}042 = 0.391 < 1$ (OK)

$$q_t = \frac{P+W}{L_{eff}B} = \frac{65{,}000+2291.67}{5.932*4} = 2{,}836 \text{ psf}$$

$q_t/q_a = 2836/3000 = 0.945 < 1$ (OK)

Since all utilization ratios are smaller than 1, the mat is acceptable for this application.

All three methods agree that the mat is acceptable for this application.

CHAPTER 6: CONCLUSIONS AND FUTURE RESEARCH

6.1. Conclusions and Observations

A detailed nonlinear finite element model was developed to predict the behavior and performance of Cross Laminated Timber (CLT) mats. The effectiveness of the FEA model has been verified against experimental data performed done by Mahamid et al. (2017) [2]. The following conclusions and observations were achieved in this study:

1. Good agreement was achieved between the finite element and experimental results. The proposed FEA can be used to determine maximum deflections, shear and normal stresses.
2. Orthotropic elastic model for wood and nonlinear damage material model used were found to be appropriate to simulate the behavior of CLT members.
3. The CLT mats, tested to failure, failed mostly in bending and not in shear due to the bending stresses exceeding the specified reference ultimate values.
4. The CLT adhesives were initially included in the non-linear CLT model. It was observed that adhesives do not fail prior to wood and since they did not influence the analysis results due to their insignificant thickness, bonded contact interfaces were used to simulate the behavior between CLT layers.
5. A comparative analysis was performed between CLT and traditional wood mats. 5-ply and 7-ply CLT mats reached failure at a higher load than a traditional heavy timber wood mat connected by steel rods along the length of the mat. This application highlights one of the many benefits of using CLT over traditional wood mat, which contradicts with current industrial practices published guides that do not recommend the use of CLT as mats. This research eliminates such limitations for mat applications.

6. A CLT design procedure was proposed and in order to achieve this objective, a nonlinear finite element wood model supported by soft soil such as low plasticity clay, was developed to compare with the results of the crane mat arrangement used in the "Mobile crane support handbook" (Duerr, 2015) [7]. The finite element results were in good agreement with Duerr's procedure's results. After proving the reliability of the FE model, modifications were proposed to current design procedures.
7. The developed CLT design procedure for mats focuses on the effective section properties of CLT per Shear Analogy method [1]. Three different design methods were adapted to check the capacity of such mats under different loads and different ground bearing capacities.

6.2. Future work

1. The proposed design procedure is based on three different methods considering 3-, 5- and 7-ply CLT mats. More configurations can be investigated to further check the adequacy of the mats as well as compare the accuracy of the methods used.
2. 2. Perform an extensive study on different configurations of CLT mats supported by different types of soil under different load cases. This would require the testing of many FEA models to draw conclusions on the behavior and failure modes of soil and CLT mats.
3. Investigate different types of adhesives used in CLT members
4. Investigate different types of wood species to improve durability of members for mat applications

REFERENCES

1. CLT Handbook, FPI Innovations, *USA Edition*, Quebec, Canada 2013

2. Mahamid,M., Brindley,T., Triandafilou,N., Domagala, S., "Behavior & Strength Characteristics of Cross-Laminated Timber Mats: Experimental and Numerical Study", *Structures Congress*, USA 2017

3. Forest Product Laboratory ,United States Department of Agriculture, "Wood Handbook, Wood as an Engineering Material ", FPL-RP-531,1994

4. ANSYS Inc., "Ansys Theory Manual Release 5.6 11th edition", 1999

5. ANSI/APA PRG 320-2012, "Standard for Performance-Rated Cross-Laminated Timber", 2012

6. American Wood Council, "Supplement NDS (National Design Specification), Design Values for Wood Construction", 2011

7. Duerr, D., "Mobile Crane Support Handbook", 2015

8. CAE Associates, "Progressive Damage of Fiber Reinforced Composites in ANSYS V.15.0", 2014

9. Autodesk Helius PFA, Alternative Failure Criteria, 2016 (https://knowledge.autodesk.com)

10. Drucker, D.C. , Prager, W. "Soil Mechanics and Plasticity Analysis or Limit Design", *Quarterly of Applied Mathematics*, Vol. 10, No. 2, pp. 157-165, 1952

11. Bartlett, S., "Mohr Coulomb Model", Numerical Methods in Geotechnical Engineering, The University of Utah, 2010

12. Boldyrev, G.G, Muyzemnek, A.J, "The modeling of Deformation Process in Soils with use of Ansys and Ls-Dyna Programs",*International Conference on Case Histories in Geotechnical Engineering*, 2008

13. Rakic,D., Miroslav,Z., "Stress Integration of the Drucker Prager material model with kinematic hardening",*Theoretical and Applied mechanics*, Voume 42, pp 201-209, 2015

14. Balmer, G., "A general analytical solution for Mohr's envelope", *Proceedings of American Society for Testing and Materials 52*, pp.1260–1271, 1952

15. Geotechdata.info, Cohesion, Young's Modulus, Posison's Ratio, 2008 (http://geotechdata.info)

16. Kowalska, M., "Influence of the Ratio between dilatancy angle and internal friction angle on stress distribution behind a gravity retaining wall", 2015

17. Lehringer, C., "Purbond 2C-adhesives", Cost Action FP 1004, Wrozlaw 2012

18. FreelinWade, Polyurethane Technical Material Data Sheet, McMinnville, 2006

19. Wahab, Magd Abdel, "The Mechanics of Adhesives in Composite and Metal Joints", 2014

20. Hindman, D.P., Lee, J. N., "Modeling Wood Strands as Multi-Layer Composites: Bending and Tension Loads", *Journal of Wood and Fiber Science*, 39(4), pp.515-526, 2007

21. Moses, D. , Prion, H., "Anisotropic Plasticity and Failure Prediction in Wood Composites", 2002

22. Tankut, N., Tankut, A., Zor M., "Finite Element of Wood Materials", 2014

23. Mackerle, J., "Finite Element Analyses in wood research: a bibliography", September 2005

24. O'Brien, M. , "Finite Element Analysis of Wood and Composite Structured Hockey Sticks", 2003

25. Colakoglu, M., Apay A., "Finite Element Analysis of wooden chair strength in free drop", *International Journal of the Physical Sciences* Vol. 7(7), pp.1105-1114, 2012

26. CLT Handbook, FPI Innovations, *Canadian Edition*, Quebec, Canada 2011

27. Stoeckel, F., Konnerth, J., "Mechanical properties of adhesives for bonding wood", *International Journal of Adhesion and Adhesives* 45:32-4, 2013

28. Adams, R.D., Comyn. J. , "Structural Adhesive Joints in Engineering", 1997

29. Chi, L., Kushwaha R.L. ,"Finite element analysis of soil forces on two shapes of tillage tool", 1991

30. Ravishankar, P., Satyam, N., " Finite Element Modeling to Study soil structure interaction of asymmetrical tall building", *International Journal of Science and Technology and Engineering*, Volume 3, Issue 11, 2013

31. Gillholm, V., Rosander, I., "Evaluation of plastic mats as access roads", Chalmers University of Technology, Goteborg, Sweden 2014

32. Guindos, P., Guaita, M., “A three-dimensional wood material model to simulate the behavior of wood with any type of knot at the macro-scale”, *Wood Science and Technology 47(3)*, 2012

33. Soil Strength Parameters, Rocscience Geotechnical Software, 1996 (https://www.rocscience.com)

34. ANSYS, Inc., ANSYS Mechanical APDL Element Reference, 2016

VITA

Ms. Ines Torra graduated from University of Illinois at Chicago with a Bachelor's of Science in Biomechanical Engineering. Ms. Torra is currently a graduate student at University of Illinois at Chicago in the Department of Civil and Materials Engineering. She worked on developing a design procedure for Cross Laminated Timber members as her Master's Thesis project and will earn Master of Science Degree from University of Illinois at Chicago in 2017. In the future, she will pursue a Doctorate Degree in the field of Structural Engineering.